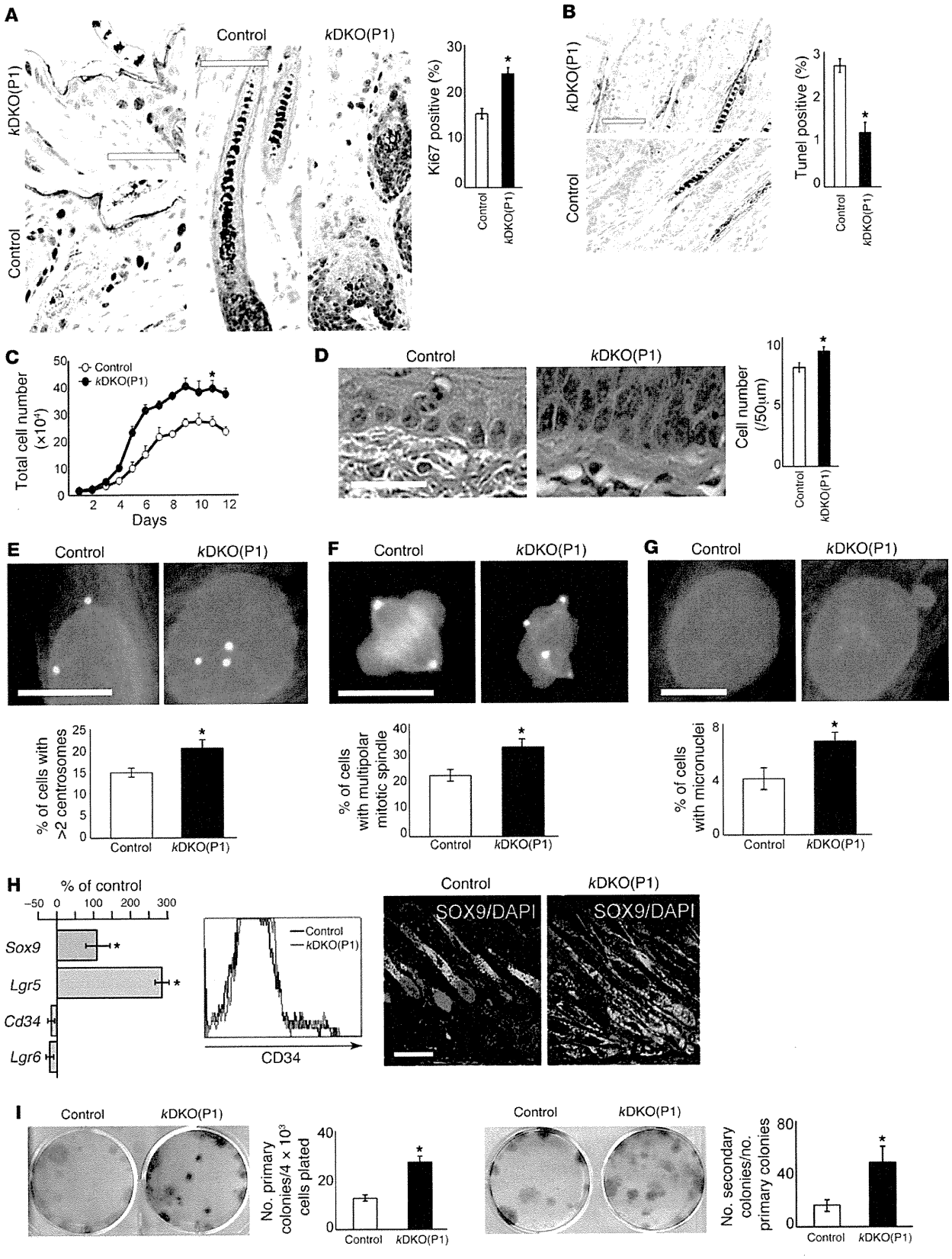
A
Control
kDKO(P1)
kDKO(P1)
Control
Ki67 positive (%)
30
20
10
0
*
Control
kDKO(P1)
B
kDKO(P1)
Control
Tunel positive (%)
3
2
1
0
*
Control
kDKO(P1)
C
Control
kDKO(P1)
Total cell number (×10⁴)
50
40
30
20
10
0
*
2
4
6
8
10
12
Days
D
Control
kDKO(P1)
Cell number (/50μm)
10
5
0
*
Control
kDKO(P1)
E
Control
kDKO(P1)
% of cells with >2 centrosomes
25
20
15
10
5
0
*
Control
kDKO(P1)
F
Control
kDKO(P1)
% of cells with multipolar mitotic spindle
40
30
20
10
0
*
Control
kDKO(P1)
G
Control
kDKO(P1)
% of cells with micronuclei
8
4
0
*
Control
kDKO(P1)
H
% of control
−50
0
100
200
300
Sox9
Lgr5
Cd34
Lgr6
*
*
Control
kDKO(P1)
CD34
Control
kDKO(P1)
SOX9/DAPI
SOX9/DAPI
I
Control
kDKO(P1)
No. primary colonies/4 × 10³ cells plated
40
20
0
*
Control
kDKO(P1)
Control
kDKO(P1)
No. secondary colonies/no. primary colonies
80
40
0
*
Control
kDKO(P1)

Figure 4

Tumorigenic anomalies in *Mob1a/1b* double-homozygous mutant keratinocytes. (**A**) Anti-Ki67 immunostaining of IFE (left) and HF (middle) of control and *k*DKO(P1) mice at P13. Scale bars: 50 μm. Quantitation of Ki67$^+$ cells (right); $^*P < 0.01$. (**B**) Histology (left) and quantitation (right) of TUNEL-stained cells in epidermis from control and *k*DKO(P1) mice at P16. Scale bar: 50 μm; $^*P < 0.01$. (**C**) Keratinocytes from control and *k*DKO(P1) mice at P4 were cultured for the indicated number of days, and total cell numbers were counted. *k*DKO(P1) keratinocytes achieved higher saturation plating density; $^*P < 0.01$. (**D**) Left: H&E-stained epidermal basal layer of control and *k*DKO(P1) mice at P19. Scale bar: 20 μm. Right: quantitation (cell number/50 μm BM); $n = 5$/group; $^*P < 0.05$. (**E–G**) Immunostaining to detect γ-Tubulin (green) and α-Tubulin (red) in control and *k*DKO(P1) keratinocytes. DAPI, nuclei. Mutant keratinocytes showed excess centrosomes (**E**), multi-polar spindles (**F**), and micronuclei (**G**). Scale bars: 20 μm; $^*P < 0.05$. (**H**) Identification of keratinocyte stem cells in HFs of control and *k*DKO(P1) mice at P19 ($n = 4$/group) using quantitative RT-PCR (left), $^*P < 0.01$; flow cytometry (middle) to detect CD34; immunostaining (right) to detect SOX9. Scale bar: 100 μm. (**I**) Freshly isolated control and *k*DKO(P1) keratinocytes were plated to generate primary colonies (left) and secondary colonies (right). Giemsa staining (top) and colony counts (bottom) were performed on day 14 after plating; $n = 4$/group; $^*P < 0.02$. Results shown are representative of at least 3 independent trials and at least 3 mice/group. Data are presented as the mean ± SEM, and *P* values were determined using the 2-tailed Student's *t* test.

resis (Figure 5E). These data show that MOB1 regulates LATS1/2-YAP1 signaling essential for mammalian skin homeostasis.

MOB1 is involved in the onset of malignant outer root sheath tumors resembling trichilemmal carcinomas. Microscopic analysis of the skin tumors of $Mob1a^{\Delta/\Delta}1b^{tr/+}$ and $Mob1a^{\Delta/+}1b^{tr/tr}$ mice revealed lesions consisting of invasive epithelial lobules with atypical cytology, an increased number of mitotic cells, and horn cysts (Figure 6A). Trichilemmal keratinization and continuity with the follicular epithelium (Figure 6A) were focally evident. Because these features are characteristic of trichilemmal carcinomas of outer root sheath origin, we immunostained these tumors with Abs recognizing KRT17, KRT5, KRT15, KRT10, Trichohyalin, or AE13. All tumors were positive for KRT17 (outer root sheath marker), KRT5 (basal cells and outer root sheath), and KRT15 (basal cells, outer root sheath, and bulge), but negative for KRT10 (upper basal IFE) and Trichohyalin (inner root sheath) (Figure 6B). Some tumors were also positive for AE13 (hair shaft marker), confirming that these malignancies were derived from the HF outer root sheath. Thus, deficiency for the Hippo signaling element MOB1 in mice leads to tumors with the features of trichilemmal carcinomas.

In humans, the most common HF-derived carcinomas are nodular BCCs, which are driven by hyperactivated SHH signaling (5). However, immunoblotting of our MOB1-deficient keratinocytes showed that neither GLI2 (downstream effector in the SHH pathway) nor the LEF1 or HES1 proteins important for HF morphogenesis were elevated (Figure 6C). In addition, while AKT was not activated in the mutant keratinocytes, phospho-ERK was increased (Figure 6C). To rule out the involvement of the SHH pathway in tumorigenesis linked to MOB1 deficiency, we immunostained control and mutant keratinocytes with Abs validated to detect GLI2 or GLI1 (Supplemental Figure 10, A and B) in patterns consistent with a previous report (40). However, when we immunostained control and *k*DKO(P1) keratinocytes with these Abs, no differences were detected (Figure 6D and Supplemental Figure 10C). Furthermore, GLI2 levels in 4 trichilemmal carcinoma samples from *k*DKO (P1) mice were not obviously increased compared with GLI2 levels in cultured control keratinocytes (Figure 6E). Thus, the SHH pathway involved in nodular BCCs does not appear to be driving the development of the trichilemmal carcinomas arising in the absence of MOB1A/1B.

In humans, trichilemmal carcinomas are very rare and composed mainly of basaloid and squamous cells, with some clear cells (Figure 6F). We performed immunostaining to detect YAP1 in samples of 14 human trichilemmal carcinomas with accompanying noncancerous epidermis. We found that, in noncancerous skin, YAP1 was expressed in the nuclei of IFE basal cells and HF outer root sheath cells (Figure 6G). Strikingly, a significant proportion (11/14, 79%) of trichilemmal carcinomas showed an increase in total YAP1$^+$ cells (Figure 6G and Table 3). Almost as many (10/14, 71%) trichilemmal carcinomas exhibited elevated nuclear YAP1 within the tumor mass (Figure 6G and Table 3). In addition, when immunostained to detect MOB1A/1B, half of trichilemmal carcinomas examined (5/10, 50%) showed decreased MOB1A/1B expression (Figure 6G and Table 3). Moreover, 10/10 (100%) of these cases in which MOB1 was decreased displayed elevated nuclear YAP1 within the tumor. These data support our hypothesis that it is the mammalian Hippo pathway, rather than the SHH pathway, that is involved in the onset of non-BCC follicular cancers such as trichilemmal carcinomas.

Discussion

We have demonstrated that mice completely deficient for *Mob1* have the most severe phenotype among strains lacking a Hippo signaling component. *Mob1a/1b* double-homozygous-null mutant mice die at gastrulation, much earlier than mice lacking *Mst1/2* (15), *Lats2* (21), *Lats1* (14), *Sav1* (20), or *Nf2* (19). Our data further indicate that MOB1 is essential for embryogenesis and that functions of MOB1A and MOB1B overlap. In addition, the tumor spectrum observed in heterozygous *Mob1*-deficient mice is the broadest among mutants lacking Hippo components. These findings suggest both that MOB1 is the key molecule in the Hippo signaling pathway and that MOB1 may have molecular target(s) other than the Hippo pathway. This notion is consistent with the reduced expression or mutation of MOB1 frequently observed in a variety of human cancers (17, 33, 34), and with MOB1's reported binding to a range of molecules, including TSSC1, NUP98, HDAC3, and DIPA (CCDD85B) (41, 42). Our results also imply that MOB1A may be more important than MOB1B, at least for embryogenesis and liver homeostasis, because *Mob1b* heterozygotes lacking *Mob1a* show partial embryonic lethality (Supplemental Table 1) and develop liver cancers (Table 2), whereas *Mob1a* heterozygotes lacking *Mob1b* are all viable and free of liver tumors.

The lethality of *Mob1*-deficient mice may stem from their failure to form primitive endoderm. The endodermal markers *Pdgfra* and *Gata4* were markedly reduced in *Mob1*-deficient cells, whereas the primitive ectoderm markers *Nanog*, *Sox2*, *Fgf5*, and *Pax6* were normal. Our mutant showed abnormal YAP1 activation, and activated YAP1 normally activates the transcription factor TEAD2. TEAD2 regulates primitive endoderm-specific genes such that sustained inhibition of TEAD2 enhances primitive endoderm-specific gene expression (43). YAP1 and TEADS reportedly increase the expression of pluripotency genes such as *Oct3/4* and *Sox2* (43, 44), as well as the trophoblast gene *Cdx2* (45, 46). However, levels of Oct3/4, SOX2, and CDX2 proteins were normal in our *Mob1*-deficient embryos. Thus, although we found YAP1 to be activated in the

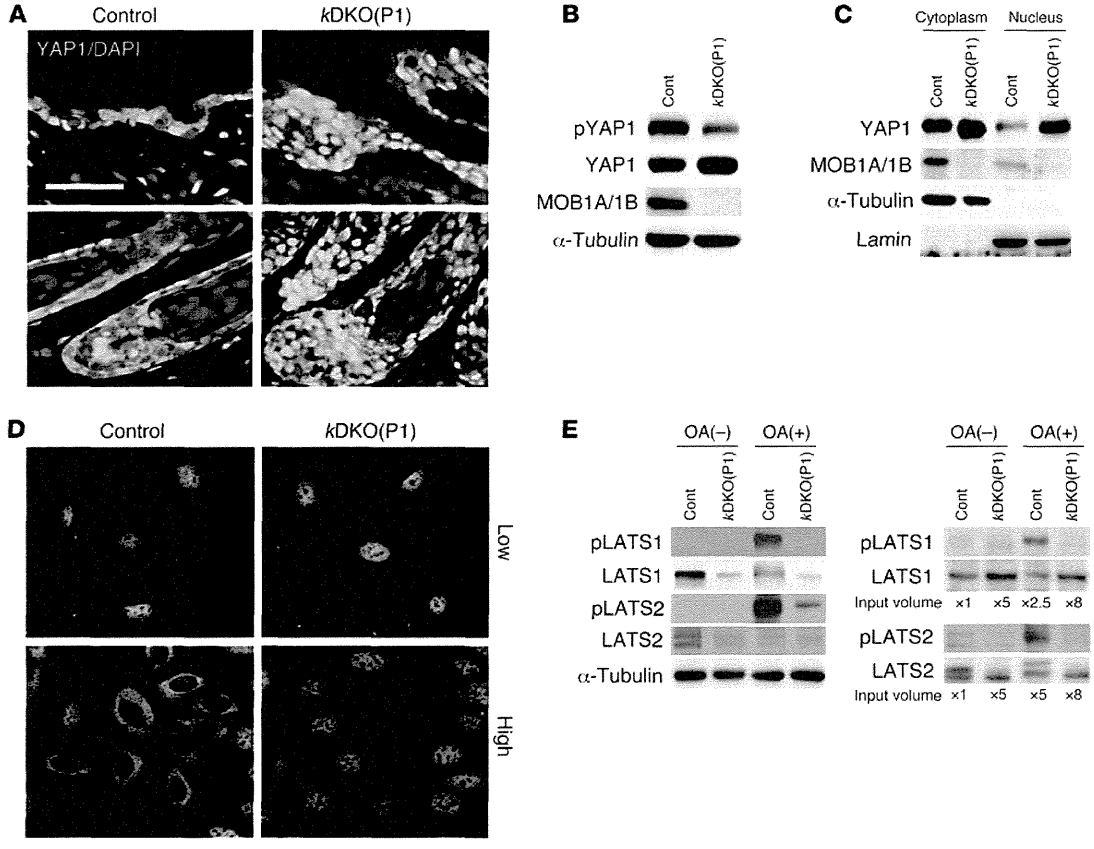

Figure 5

MOB1-mediated regulation of the LATS1/2-YAP1 pathway controls skin homeostasis. (**A**) Immunostaining of keratinocytes from control and *k*DKO(P1) mice at P19 to detect YAP1 in the IFE (top) and HF (bottom). Scale bar: 50 μm. (**B**) Immunoblot of total extracts of control and *k*DKO(P1) keratinocytes to detect the indicated proteins. α-Tubulin, loading control. (**C**) Immunoblot of cytoplasmic and nuclear fractions of control and *k*DKO(P1) keratinocytes to detect the indicated proteins. α-Tubulin and Lamin, cytoplasmic and nuclear loading controls, respectively. (**D**) Immunostaining to detect YAP1 in keratinocytes from control and *k*DKO(P1) mice plated at low or high cell density. YAP1 is localized in the nucleus in mutant keratinocytes even at high cell density. (**E**) Immunoblot to detect the indicated proteins in total extracts of control (Cont) and *k*DKO(P1) keratinocytes that were left untreated (OA–) or treated with OA (OA+). Left: unadjusted lysates. Right: levels of LATS1 and LATS2 proteins in each sample were adjusted to equality before electrophoresis. Results shown are representative of at least 3 independent trials and at least 3 mice/group.

mutant ICM, a much stronger alteration of YAP1 activity may be necessary to induce a detectable effect on these genes.

We have shown that, in contrast to MST1/2 and LATS1/2, MOB1 is a potent tumor suppressor in a range of tissue types that includes the skin. All cancers examined in $Mob1a^{\Delta/+}1b^{tr/tr}$ and $Mob1a^{\Delta/\Delta}1b^{tr/+}$ mice had lost the WT *Mob1* allele, suggesting increased genetic instability. *Mob1a/1b* mRNAs and proteins are frequently cosuppressed in tumor cell lines (data not shown), and the MOB1A and MOB1B amino acid sequences are 95% identical. We are currently clarifying whether a common mechanism regulates these 2 genes.

In our $Mob1a^{\Delta/+}1b^{tr/tr}$ and $Mob1a^{\Delta/\Delta}1b^{tr/+}$ mice, the most frequent tumors were malignant outer root sheath tumors resembling trichilemmal carcinomas (Figure 6A). Histologically, these malignancies were not BCCs because they lacked the cellular palisading typical of BCCs (4). Moreover, cultured *Mob1a/1b* double-mutant keratinocytes did not show the SHH pathway activation important for BCC onset (Figure 6C). Benign trichilemmomas are frequently observed in Cowden disease patients with hereditary PTEN mutations (47), but these tumors seldom become malignant. The trichilemmal growths in our *Mob1*-deficient mutants were clearly cancerous but showed no activation of the PTEN effector AKT (Figure 6C). Importantly, like our mutant mouse tissues, our human trichilemmal carcinoma samples exhibited frequent MOB1A/1B inactivation and YAP1 activation (Figure 6G and Table 3). These findings suggest that impaired Hippo signaling may drive trichilemmal carcinoma onset in humans.

Mob1-deficient keratinocytes exhibit enhanced proliferation, apoptotic resistance, impaired contact inhibition, increased centrosomes, accelerated mitotic exit, and enhanced progenitor self-renewal. In addition, polarity must be defective without MOB1 because (a) KRT15$^+$ cells were scattered inside the IFE and not localized to the basal layer; (b) CD34$^+$ bulge stem cells were not localized in the bulge; and (c) hair bundles in the organ of Corti were disorganized (Supplemental Figure 2B). To date, 2 transgenic mouse strains overexpressing *Yap1* in the skin have been described (23, 48). Like our *Mob1* mutants, *Yap1* transgenic mice show hyperplastic IFE. However, these latter animals also have a severe defect in HF

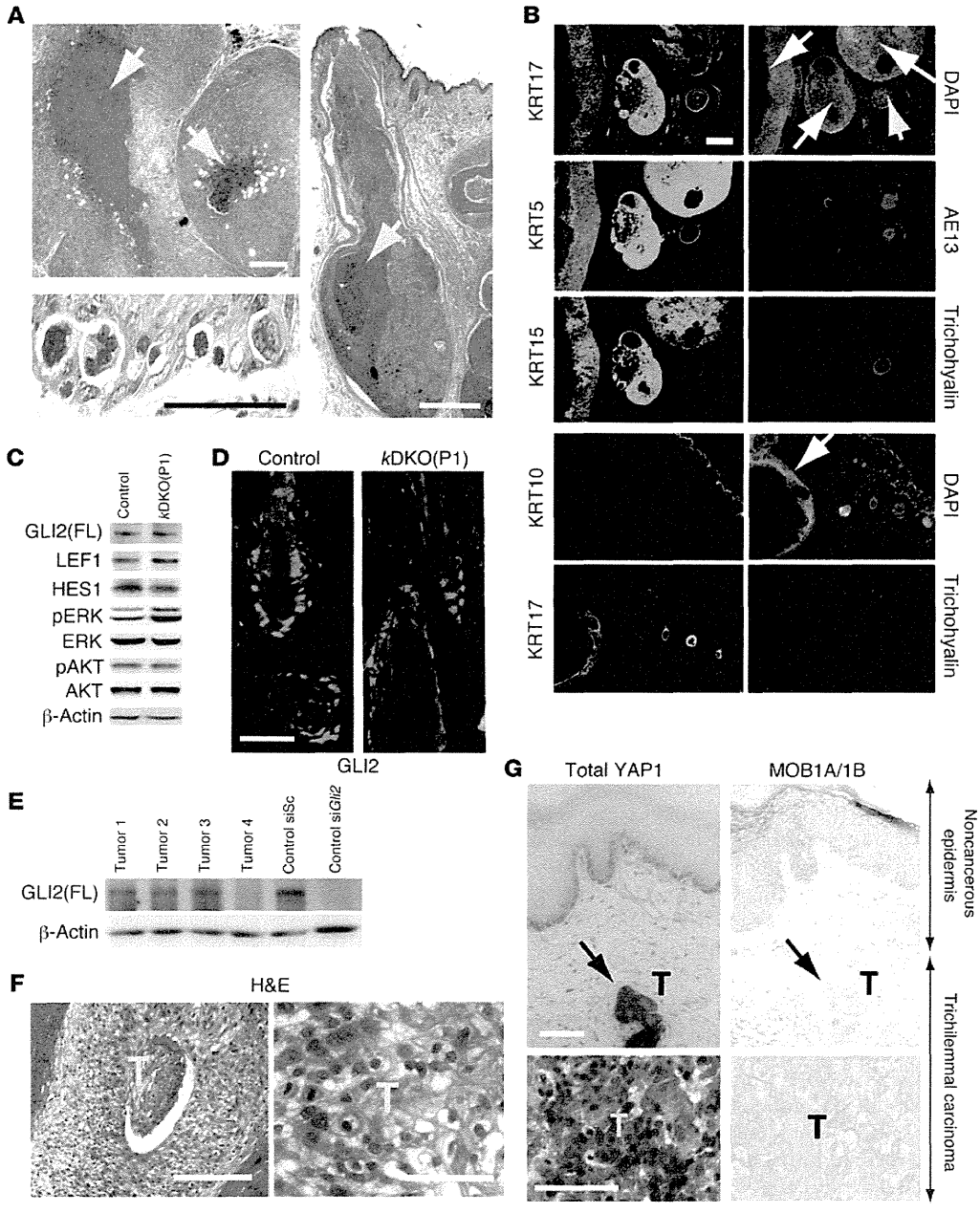

Figure 6

Characterization of skin cancers of *Mob1*-deficient mice and human trichilemmal carcinomas. (**A**) H&E-stained sections of representative tumors from *Mob1a*$^{\Delta/\Delta}$*1b*$^{tr/+}$ or *Mob1a*$^{\Delta/+}$*1b*$^{tr/tr}$ mice showing: (top left) characteristic trichilemmal keratinization (yellow arrows; also in right); (bottom left) atypical and highly mitotic cells; and (right) continuity with the epidermis. Scale bars: 50 μm (left); 500 μm (right). (**B**) Immunostaining of tumors from *Mob1a*$^{\Delta/\Delta}$*1b*$^{tr/+}$ or *Mob1a*$^{\Delta/+}$*1b*$^{tr/tr}$ mice to detect the indicated skin markers. White arrows, cancerous lesions; yellow arrow, nontumorous HF. Scale bar: 200 μm. (**C**) Immunoblot of total extracts of control and *k*DKO(P1) keratinocytes to detect ERK and AKT activation as well as the HF morphogenesis proteins GLI2 (FL; full length), LEF1 and HES1. β-Actin, loading control. (**D**) Immunostaining to detect GLI2 in HFs from control or *k*DKO(P1) mice. Scale bar: 25 μm. (**E**) Immunoblot to detect GLI2 in total extracts of control keratinocytes transfected with scramble siRNA (Control siSc) or *Gli2* siRNA (Control si*Gli2*), as well as in samples of 4 trichilemmal carcinomas (Tumor 1, 2, 3, 4) from *k*DKO(P1) mice. (**F**) H&E staining of a human trichilemmal carcinoma viewed at low (scale bar: 200 μm) or high magnification (scale bar: 50 μm). (**G**) Immunostaining to detect YAP1 and MOB1A/1B in human trichilemmal carcinomas and nearby noncancerous tissues. Top: Both noncancerous and trichilemmal carcinoma (T) tissues can be seen in low-magnification images. Bottom: High-magnification images of human trichilemmal carcinomas. Scale bars: 100 μm. Results shown are representative of at least 3 independent trials and at least 3 mice/group.

Table 3
Quantitation of human trichilemmal carcinoma samples showing an increase in YAP1+ cells and/or elevation in nuclear YAP1, and a decrease in MOB1A/1B

	Increased YAP1	Nuclear accumulation of YAP1	Decreased MOB1A/1B
Trichilemmal carcinoma	11/14 (79%)	10/14 (71%)	5/10 (50%)

formation. This difference may account for the development of IFE-derived squamous cell carcinomas in *Yap1* transgenic mice, but HF-derived trichilemmal carcinomas in *Mob1*-deficient mutants.

At the biochemical level, *Mob1*-deficient keratinocytes exhibited reductions in not only phospho-LATS1/2, but also total LATS1/2 proteins. *Lats1/2* mRNAs were comparable in control and mutant keratinocytes (data not shown), indicating that this surprising decrease in LATS1/2 proteins occurs posttranscriptionally. Like MOB1, SAV1 is a scaffolding protein in the Hippo pathway, but unlike *Mob1* deficiency, *Sav1* deficiency decreases phospho-MST, but does not affect total MST or LATS1/2 proteins (20). Another interesting biochemical observation was the activation of ERK in our *Mob1*-deficient keratinocytes: no connection between MOB1 and ERK has been reported to date. With respect to Hippo signaling, ERK can be activated by YAP1 (49) or suppressed by NF2 (50) or MST2 (51). Since NF2 and phospho-MST1/2 were not decreased in our *Mob1*-deficient keratinocytes (data not shown), we speculate that the increased YAP1 in these cells may have triggered their abnormal ERK activation.

Because all of our *Mob1a/1b*-deficient mice spontaneously developed tumors (and especially trichilemmal carcinomas), we believe that the loss of MOB1A/1B helps to both initiate and promote carcinoma onset. With respect to tumor initiation, the observed increase in the number of centrosomes and/or micronuclei in our mutant cells may have introduced detrimental alterations into their DNA. With respect to cancer promotion, the enhanced proliferation, apoptotic resistance, impaired contact inhibition, and increased progenitor self renewal associated with loss of MOB1A/1Bmay support the growth and progression of cells that have undergone tumor initiation events.

The very rare occurrence of trichilemmal carcinomas in humans has slowed the identification of genes involved in their development. Expression levels of MOB1A, LATS1/2, and SAV1 are more frequently reduced in the advanced stages of colon (33), breast (52), and renal cancers (53) than in the early stages of these malignancies. In lung cancers, the reverse is true, since MOB1A levels are frequently lower in the early pT1 stage of non–small-cell lung cancer as compared with later stages (34). These observations suggest that the loss of Hippo signaling molecules can be an important driver of cancer progression in humans. Further study of alterations to gene or protein expression or functions of Hippo signaling components in a broad range of human malignancies may increase our understanding of their involvement in tumorigenesis.

In conclusion, our results demonstrate that (a) MOB1 is a broadly-acting tumor suppressor in mice and (b) Hippo signaling drives trichilemmal carcinoma onset in the skin. Therapeutic strategies to control Hippo signaling or MOB1 expression might therefore benefit many cancer patients, particularly those with HF-derived cancers.

Methods

Generation of Mob1a^{flox} and Mob1b^{tmp} mice. A conditional targeting vector based on the Cre-loxP system was constructed to delete a genomic fragment containing exon 2 of the murine *Mob1a* gene (Supplemental Figure 1). This deletion generates a frame shift and early stop codon in exon 3. We introduced 1 *loxP* site into *Mob1a* intron 1 and 2 *loxP* sites into intron 2 to flank *Mob1a* exon 2. The *PGK-Hyg* resistance cassette was inserted in antisense orientation between the 2 *loxP* sites in intron 2. The resulting targeting vector was electroporated into E14K ES cells, and homologous recombinants were confirmed by Southern blotting using 5′ flanking probe A and a *Hyg*-specific probe. Correctly targeted *Mob1a* mutant clones were transiently transfected with *pMC1-Cre* (54) to delete the *loxP*-flanked *Hyg^r* gene. Progeny clones sensitive to hygromycin were subjected to Southern blotting to identify those retaining exon 2 flanked by 2 *loxP* sites (the *Mob1a^{flox}* allele) and those lacking exon 2 (*Mob1a$^{\Delta}$* allele; equivalent to a knockout mutation). For *Mob1b*-deficient mice, an ES cell line bearing a gene trap mutation of intron 2 of the *Mob1b* gene was obtained from the Sanger Institute (Hinxton, United Kingdom). The single integration of the trapped site was confirmed by PCR and genomic Southern blotting using 5′ flanking probe C and a neospecific probe. *Mob1a^{flox}*, *Mob1a$^{\Delta}$*, and *Mob1b^{tmp}* mice were generated from ES cell clones using standard procedures and backcrossed to C57BL/6 mice 3 times before intercrossing to generate *Mob1a$^{fl/fl}$*, *Mob1a$^{\Delta/\Delta}$*, and *Mob1b$^{tr/tr}$* progeny. Primers used for genotyping are listed in Supplemental Table 2.

In vitro culture of preimplantation embryos. E3.5 embryos derived from the intercrossing of *Mob1a$^{\Delta/+}$1b$^{tr/tr}$* males and females were analyzed as described (55). Briefly, blastocysts were individually cultured in 24-well plates in ES cell medium without LIF and photographed every 24 hours. On day 8, the morphology of each embryo was recorded and its genotype determined by PCR.

Embryo immunostaining. Immunofluorescent staining of embryos was performed as described (45). Briefly, embryos (E3.5) were cultured overnight prior to fixation in 4% paraformaldehyde. Fixed tissues were permeabilized with 0.2% Triton X-100, blocked with 2% goat serum, and incubated overnight at 4°C with Abs recognizing CDX2 (Biocare Medical), Oct3/4 (gift of H. Niwa, Riken), PDGFRα (eBiosciences), GATA4/6 (Santa Cruz Biotechnology Inc.), NANOG (ReproCELL), Troma-1 (DSHB), SOX2 (Abcam), or YAP1 (Sigma-Aldrich). Secondary Abs were Alexa Fluor 488 goat anti-rabbit or Alexa Fluor 568 goat anti-mouse (Molecular Probes). Nuclei were visualized using DAPI (Dojindo). Stained embryos were examined by confocal microscopy.

Generation and differentiation of Mob1a/1b double-mutant ES cells. ES cells established from embryos derived from *Mob1a$^{fl/fl}$1b$^{tr/tr}$* intercrosses were transfected with linearized *CMV-Mer-Cre-Mer* plasmid DNA (56) plus *pApuro2* (57). To generate *ERCreMob1a$^{fl/fl}$1b$^{tr/tr}$* ES clones, ES cells were selected by culture for 12 days in complete ES cell medium containing 1 μg/ml puromycin (Invivogen) on an irradiation-inactivated Puro MEF feeder layer. Tamoxifen (3.3 μM; Toronto Research Chemicals) was added (or not) for 2 days to completely delete the *Mob1a* gene (data not shown). Control and mutant EBs were generated from hanging drops of approximately 1,000 ES cells/20 μl medium as described (58).

Generation of keratinocyte-specific Mob1a/Mob1b double-mutant mice. *Mob1a$^{fl/fl}$1b$^{tr/tr}$* mice were mated to *Krt14CreER* transgenic mice (35) in which Cre can be activated by tamoxifen under the control of the *Krt14* promoter. Offspring carrying *Krt14CreER* plus 2 copies of the floxed *Mob1a* allele (*Mob1a$^{fl/fl}$*) and 2 copies of the trapped *Mob1b* allele (*Mob1b$^{tr/tr}$*) were administered tamoxifen and used in the analysis as homozygous double mutant (*Krt14CreERMob1a$^{fl/fl}$1b$^{tr/tr}$* +tamoxifen; *k*DKO) mice.

Krt14CreERMob1a$^{fl/fl}$*1b*$^{tr/tr}$ mice without tamoxifen and *Mob1a*$^{+/+}$*1b*$^{tr/tr}$ or *Mob1a*$^{+/+}$*Mob1b*$^{tr/tr}$ mice with tamoxifen but without *Krt14CreER* were indistinguishable in pilot experiments examining histology and MOB1 protein levels. *Krt14CreERMob1a*$^{fl/fl}$*1b*$^{tr/tr}$ mice without tamoxifen were arbitrarily chosen to serve as controls. To induce Cre in keratinocyte stem/progenitor cells, P1 mice were intraperitoneally administered 0.2 mg tamoxifen on that one day, or P28 mice received 0.5 mg tamoxifen each day for 7 days starting on P28.

Characterization of primary keratinocytes. Primary keratinocytes isolated from control and *k*DKO mice were cultured as described (59). For cell saturation density assays, keratinocytes at passage 2 were seeded in type I collagen–coated 24-well plates (0.3×10^5/well) and cultured for up to 12 days before counting cell numbers. For colony-forming assays, keratinocytes at passage 1 were seeded in 6-well plates (0.4×10^4/well). After 2 weeks, half the wells were fixed and stained with Giemsa (Muto Pure Chemicals), and the number of primary colonies was counted. Keratinocytes of an unfixed well were then trypsinized and reseeded so that each well of a 6-well plate received cells from 1 primary colony. Reseeded cells were cultured for 2 weeks to generate secondary colonies.

Clinical samples. Surgically obtained trichilemmal carcinoma samples containing noncancerous tissues were acquired from the Department of Regenerative Dermatology (Osaka University). Resected cancer tissues were fixed in formalin and stained with anti-YAP1 Ab (Cell Signaling) and anti-MOB1A/1B Ab (AP7031b; Abgent) using a standard protocol.

Statistics. KaleidaGraph software was used for statistical analyses. Data are shown as the mean ± SEM, and P values were determined using the 2-tailed Student's t test unless otherwise stated. $P < 0.05$ was considered statistically significant.

Study approval. The clinical sample study design was approved by the Institutional Review Board of Osaka University, and written informed consent was obtained from all patients. All animal experiments were approved by the Animal Experiment Review Boards of Kyushu University and Akita University.

See Supplemental Methods for additional details.

Acknowledgments

We are grateful to S. Kuroda, Y. Horie, M. Natsui, H. Takahashi, and K. Enomoto (all of Akita University); to M. Fukumoto (of Tohoku University); to H. Konishi, A. Fujimoto, M. Suzuki, C. Meno, and Y. Oda (all of Kyushu University); and to K. Katsuoka (of Kitasato University) for expert technical support and helpful discussions. In addition, we thank B. Vanhaesebroeck (Barts Cancer Institute, London, United Kingdom) for critical reading of the manuscript. This work was supported by grants from the Ministry of Education, Culture, Sports and Technology of Japan (MEXT); the Cooperative Research Project Program of the Medical Institute of Bioregulation, Kyushu University; the Uehara Memorial Foundation; the Takeda Medical Foundation; the Naito Foundation; the Sumitomo Foundation; the Ono Medical Research Foundation; the Yasuda Medical Foundation; the Cosmetology Research Foundation; the Osaka Cancer Research Foundation; the Fukuoka Foundation for Sound Health; and the Astellas Foundation for Research on Metabolic Disorders.

Received for publication March 8, 2012, and accepted in revised form September 13, 2012.

Address correspondence to: Akira Suzuki, Division of Cancer Genetics, Medical Institute of Bioregulation, Kyushu University, 3-1-1 Higashiku, Higashiku, Fukuoka, Fukuoka 812-8582, Japan. Phone: 81.92.642.6838; Fax: 81.92.632.1499; E-mail: suzuki@bioreg.kyushu-u.ac.jp.

1. Blanpain C, Horsley V, Fuchs E. Epithelial stem cells: turning over new leaves. *Cell.* 2007;128(3):445–458.
2. Reya T, Morrison SJ, Clarke MF, Weissman IL. Stem cells, cancer, and cancer stem cells. *Nature.* 2001;414(6859):105–111.
3. Headington JT. Tumors of the hair follicle. A review. *Am J Pathol.* 1976;85(2):479–514.
4. Fan H, Oro AE, Scott MP, Khavari PA. Induction of basal cell carcinoma features in transgenic human skin expressing Sonic Hedgehog. *Nat Med.* 1997; 3(7):788–792.
5. Oro AE, Higgins KM, Hu Z, Bonifas JM, Epstein EH Jr, Scott MP. Basal cell carcinomas in mice overexpressing sonic hedgehog. *Science.* 1997;276(5313):817–821.
6. Edgar BA. From cell structure to transcription: Hippo forges a new path. *Cell.* 2006;124(2):267–273.
7. Harvey K, Tapon N. The Salvador-Warts-Hippo pathway – an emerging tumour – suppressor network. *Nat Rev Cancer.* 2007;7(3):182–191.
8. Hamaratoglu F, et al. The tumour-suppressor genes NF2/Merlin and expanded act through Hippo signalling to regulate cell proliferation and apoptosis. *Nat Cell Biol.* 2006;8(1):27–36.
9. Creasy CL, Chernoff J. Cloning and characterization of a human protein kinase with homology to Ste20. *J Biol Chem.* 1995;270(37):21695–21700.
10. Tao W, et al. Human homologue of the Drosophila melanogaster lats tumour suppressor modulates CDC2 activity. *Nat Genet.* 1999;21(2):177–181.
11. Valverde P. Cloning, expression, and mapping of hWW45, a novel human WW domain-containing gene. *Biochem Biophys Res Commun.* 2000; 276(3):990–998.
12. Moreno CS, Lane WS, Pallas DC. A mammalian homolog of yeast MOB1 is both a member and a putative substrate of striatin family-protein phosphatase 2A complexes. *J Biol Chem.* 2001;276(26):24253–24260.
13. Sudol M, et al. Characterization of the mammalian YAP (Yes-associated protein) gene and its role in defining a novel protein module, the WW domain. *J Biol Chem.* 1995;270(24):14733–14741.
14. St John MA, et al. Mice deficient of Lats1 develop soft-tissue sarcomas, ovarian tumours and pituitary dysfunction. *Nat Genet.* 1999;21(2):182–186.
15. Zhou D, et al. Mst1 and Mst2 maintain hepatocyte quiescence and suppress hepatocellular carcinoma development through inactivation of the Yap1 oncogene. *Cancer Cell.* 2009;16(5):425–438.
16. Tapon N, et al. Salvador promotes both cell cycle exit and apoptosis in Drosophila and is mutated in human cancer cell lines. *Cell.* 2002;110(4):467–478.
17. Lai ZC, et al. Control of cell proliferation and apoptosis by mob as tumor suppressor, mats. *Cell.* 2005; 120(5):675–685.
18. Pan D. The hippo signaling pathway in development and cancer. *Dev Cell.* 2010;19(4):491–505.
19. McClatchey AI, Saotome I, Ramesh V, Gusella JF, Jacks T. The Nf2 tumor suppressor gene product is essential for extraembryonic development immediately prior to gastrulation. *Genes Dev.* 1997; 11(10):1253–1265.
20. Lee JH, et al. A crucial role of WW45 in developing epithelial tissues in the mouse. *EMBO J.* 2008; 27(8):1231–1242.
21. McPherson JP, et al. Lats2/Kpm is required for embryonic development, proliferation control and genomic integrity. *EMBO J.* 2004;23(18):3677–3688.
22. Morin-Kensicki EM, et al. Defects in yolk sac vasculogenesis, chorioallantoic fusion, and embryonic axis elongation in mice with targeted disruption of Yap65. *Mol Cell Biol.* 2006;26(1):77–87.
23. Schlegelmilch K, et al. Yap1 acts downstream of alpha-catenin to control epidermal proliferation. *Cell.* 2011;144(5):782–795.
24. Luca FC, Winey M. MOB1, an essential yeast gene required for completion of mitosis and maintenance of ploidy. *Mol Biol Cell.* 1998;9(1):29–46.
25. Luca FC, Mody M, Kurischko C, Roof DM, Giddings TH, Winey M. Saccharomyces cerevisiae Mob1p is required for cytokinesis and mitotic exit. *Mol Cell Biol.* 2001;21(20):6972–6983.
26. Bardin AJ, Amon A. Men and sin: what's the difference? *Nat Rev Mol Cell Biol.* 2001;2(11):815–826.
27. Yoshida S, Toh-e A. Regulation of the localization of Dbf2 and mob1 during cell division of saccharomyces cerevisiae. *Genes Genet Syst.* 2001;76(2):141–147.
28. Mah AS, Jang J, Deshaies RJ. Protein kinase Cdc15 activates the Dbf2-Mob1 kinase complex. *Proc Natl Acad Sci U S A* 2001;98(13):7325–7330.
29. Hergovich A, Hemmings BA. Hippo signalling in the G2/M cell cycle phase: Lessons learned from the yeast MEN and SIN pathways. *Semin Cell Dev Biol.* 2012;23(7):794–802.
30. Chow A, Hao Y, Yang X. Molecular characterization of human homologs of yeast MOB1. *Int J Cancer.* 2010;126(9):2079–2089.
31. Stavridi ES, et al. Crystal structure of a human Mob1 protein: toward understanding Mob-regulated cell cycle pathways. *Structure.* 2003;11(9):1163–1170.
32. Bothos J, Tuttle RL, Ottey M, Luca FC, Halazonetis TD. Human LATS1 is a mitotic exit network kinase. *Cancer Res.* 2005;65(15):6568–6575.
33. Kosaka Y, Mimori K, Tanaka F, Inoue H, Watanabe M, Mori M. Clinical significance of the loss of MATS1 mRNA expression in colorectal cancer. *Int J Oncol.* 2007;31(2):333–338.
34. Sasaki H, et al. Human MOB1 expression in non-small-cell lung cancer. *Clin Lung Cancer.* 2007; 8(4):273–276.
35. Vasioukhin V, Degenstein L, Wise B, Fuchs E. The magical touch: genome targeting in epidermal stem cells induced by tamoxifen application to mouse skin. *Proc Natl Acad Sci U S A.* 1999;96(15):8551–8556.
36. Hardy MH. The secret life of the hair follicle. *Trends*

Genet. 1992;8(2):55–61.
37. Yabuta N, et al. Lats2 is an essential mitotic regulator required for the coordination of cell division. *J Biol Chem.* 2007;282(26):19259–19271.
38. Hao Y, Chun A, Cheung K, Rashidi B, Yang X. Tumor suppressor LATS1 is a negative regulator of oncogene YAP. *J Biol Chem.* 2008;283(9):5496–5509.
39. Hirabayashi S, et al. Threonine 74 of MOB1 is a putative key phosphorylation site by MST2 to form the scaffold to activate nuclear Dbf2-related kinase 1. *Oncogene.* 2008;27(31):4281–4292.
40. Mill P, et al. Sonic hedgehog-dependent activation of Gli2 is essential for embryonic hair follicle development. *Genes Dev.* 2003;17(2):282–294.
41. Ewing RM, et al. Large-scale mapping of human protein-protein interactions by mass spectrometry. *Mol Syst Biol.* 2007;3:89.
42. Rual JF, et al. Towards a proteome-scale map of the human protein-protein interaction network. *Nature.* 2005;437(7062):1173–1178.
43. Tamm C, Bower N, Anneren C. Regulation of mouse embryonic stem cell self-renewal by a Yes-YAP-TEAD2 signaling pathway downstream of LIF. *J Cell Sci.* 2011;124(pt7):1136–1144.
44. Lian I, et al. The role of YAP transcription coactivator in regulating stem cell self-renewal and differentiation. *Genes Dev.* 2010;24(11):1106–1118.
45. Nishioka N, et al. The Hippo signaling pathway components Lats and Yap pattern Tead4 activity to distinguish mouse trophectoderm from inner cell mass. *Dev Cel.* 2009;16(3):398–410.
46. Yagi R, et al. Transcription factor TEAD4 specifies the trophectoderm lineage at the beginning of mammalian development. *Development.* 2007; 134(21):3827–3836.
47. Farooq A, Walker LJ, Bowling J, Audisio RA. Cowden syndrome. *Cancer Treat Rev.* 2010;36(8):577–583.
48. Zhang H, Pasolli HA, Fuchs E. Yes-associated protein (YAP) transcriptional coactivator functions in balancing growth and differentiation in skin. *Proc Natl Acad Sci U S A.* 2011;108(6):2270–2275.
49. Kang W, et al. Yes-associated protein 1 exhibits oncogenic property in gastric cancer and its nuclear accumulation associates with poor prognosis. *Clin Cancer Res.* 2011;17(8):2130–2139.
50. Lim JY, et al. Merlin suppresses the SRE-dependent transcription by inhibiting the activation of Ras-ERK pathway. *Biochem Biophys Res Commun.* 2003; 302(2):238–245.
51. Kilili GK, Kyriakis JM. Mammalian Ste20-like kinase (Mst2) indirectly supports Raf-1/ERK pathway activity via maintenance of protein phosphatase-2A catalytic subunit levels and consequent suppression of inhibitory Raf-1 phosphorylation. *J Biol Chem.* 2010;285(20):15076–15087.
52. Takahashi Y, Miyoshi Y, Morimoto K, Taguchi T, Tamaki Y, Noguchi S. Low LATS2 mRNA level can predict favorable response to epirubicin plus cyclophosphamide, but not to docetaxel, in breast cancers. *J Cancer Res Clin Oncol.* 2007;133(8):501–509.
53. Matsuura K, et al. Downregulation of SAV1 plays a role in pathogenesis of high-grade clear cell renal cell carcinoma. *BMC Cancer.* 2011;11:523.
54. Gu H, Zou YR, Rajewsky K. Independent control of immunoglobulin switch recombination at individual switch regions evidenced through Cre-loxP-mediated gene targeting. *Cell.* 1993;73(6):1155–1164.
55. Suzuki A, et al. Brca2 is required for embryonic cellular proliferation in the mouse. *Genes Dev.* 1997; 11(10):1242–1252.
56. Verrou C, Zhang Y, Zurn C, Schamel WW, Reth M. Comparison of the tamoxifen regulated chimeric Cre recombinases MerCreMer and CreMer. *Biol Chem.* 1999;380(12):1435–1438.
57. Takata M, et al. Tyrosine kinases Lyn and Syk regulate B cell receptor-coupled Ca2+ mobilization through distinct pathways. *EMBO J.* 1994;13(6):1341–1349.
58. Sakai Y, Yoshiura Y, Nakazawa K. Embryoid body culture of mouse embryonic stem cells using microwell and micropatterned chips. *J Biosci Bioeng.* 2011;111(1):85–91.
59. Lichti U, Anders J, Yuspa SH. Isolation and short-term culture of primary keratinocytes, hair follicle populations and dermal cells from newborn mice and keratinocytes from adult mice for in vitro analysis and for grafting to immunodeficient mice. *Nat Protoc.* 2008;3(5):799–810.

Establishment of Functioning Human Corneal Endothelial Cell Line with High Growth Potential

Tadashi Yokoi[1,2], Yuko Seko[1,7], Tae Yokoi[1], Hatsune Makino[3], Shin Hatou[4], Masakazu Yamada[5], Tohru Kiyono[6], Akihiro Umezawa[3], Hiroshi Nishina[2], Noriyuki Azuma[1]*

1 Department of Ophthalomology, National Center for Child Health and Development, Tokyo, Japan, **2** Department of Developmental and Regenerative Biology, Medical Research Institute, Tokyo Medical and Dental University, Bunkyo-ku Tokyo, Japan, **3** Department of Reproductive Biology, National Research Institute for Child Health and Development, Tokyo, Japan, **4** Department of Ophthalmology, Keio University School of Medicine, Tokyo, Japan, **5** Division for Vision Research, National Institute of Sensory Organs, National Tokyo Medical Center, Tokyo, Japan, **6** Division of Virology, National Cancer Center Research Institute, Tokyo, Japan, **7** Sensory Functions Section, Research Institute, National Rehabilitation Center for Persons with Disabilities, Tokyo, Japan

Abstract

Hexagonal-shaped human corneal endothelial cells (HCEC) form a monolayer by adhering tightly through their intercellular adhesion molecules. Located at the posterior corneal surface, they maintain corneal translucency by dehydrating the corneal stroma, mainly through the Na^+- and K^+-dependent ATPase (Na^+/K^+-ATPase). Because HCEC proliferative activity is low *in vivo*, once HCEC are damaged and their numbers decrease, the cornea begins to show opacity due to overhydration, resulting in loss of vision. HCEC cell cycle arrest occurs at the G1 phase and is partly regulated by cyclin-dependent kinase inhibitors (CKIs) in the Rb pathway (p16-CDK4/CyclinD1-pRb). In this study, we tried to activate proliferation of HCEC by inhibiting CKIs. Retroviral transduction was used to generate two new HCEC lines: transduced human corneal endothelial cell by human papillomavirus type E6/E7 (THCEC (E6/E7)) and transduced human corneal endothelial cell by Cdk4R24C/CyclinD1 (THCEH (Cyclin)). Reverse transcriptase polymerase chain reaction analysis of gene expression revealed little difference between THCEC (E6/E7), THCEH (Cyclin) and non-transduced HCEC, but cell cycle-related genes were up-regulated in THCEC (E6/E7) and THCEH (Cyclin). THCEH (Cyclin) expressed intercellular molecules including ZO-1 and N-cadherin and showed similar Na^+/K^+-ATPase pump function to HCEC, which was not demonstrated in THCEC (E6/E7). This study shows that HCEC cell cycle activation can be achieved by inhibiting CKIs even while maintaining critical pump function and morphology.

Citation: Yokoi T, Seko Y, Yokoi T, Makino H, Hatou S, et al. (2012) Establishment of Functioning Human Corneal Endothelial Cell Line with High Growth Potential. PLoS ONE 7(1): e29677. doi:10.1371/journal.pone.0029677

Editor: Irina Kerkis, Instituto Butantan, Brazil

Received July 18, 2011; **Accepted** December 2, 2011; **Published** January 19, 2012

Funding: This study was supported by a grant (#18390473) from the Ministry of Education, Culture, Sports, Science and Technology (MEXT) of Japan. The funders had no role in study design, data collection and analysis, decision to publish, or preparation of the manuscript.

Competing Interests: The authors have declared that no competing interests exist.

* E-mail: azuma-n@ncchd.go.jp

Introduction

Human corneal endothelial cells (HCEC) are hexagonal in shape and form a fragile monolayer lying posterior to the surface of the cornea. These cells maintain corneal transparency by their tight intercellular barrier and perform an ion transport pump function through Na^+/K^+-ATPase, which regulates the hydration of the corneal stroma [1,2]. If HCEC sustain damage, excessive hydration and opacity of the cornea occur, resulting in decreased vision.

Corneal endothelia are believed not to increase in adult humans and in fact gradually decrease by approximately 0.5% per year [3,4,5]. Damage, injury or HCEC disease such as Fuchs' corneal dystrophy [6], diabetes [7], trauma [8], cataract surgery [9] or elevation of intraocular pressure [10] does not lead to increased proliferation but rather to an increase in cell size to compensate for the wounded area [11]. Once the cell number falls below 1,000 cells/mm^2, the monolayer of enlarged HCEC cannot maintain corneal translucency [12] and surgical treatment is required to restore vision.

Penetrating keratoplasty has long been the surgical treatment of choice, involving replacement of a total layer of cornea by donor material. However, it can also result in adverse effects such as astigmatism and severe rejection requiring long term usage of immunosuppressive drugs [13]. Recently, alternative transplantation strategies, including modified posterior lamellar keratoplasty techniques such as deep lamellar endothelial keratoplasty (DLEK) [14], Descemet's stripping with endothelial keratoplasty (DSEK) [15] and Descemet membrane endothelial keratoplasty (DMEK) [16] have been introduced to overcome these problems. Despite these advances, an increasingly aging population requiring corneal transplants and inadequate tissue quality limit the availability of donor corneas, such that alternative ways of preparing endothelial cell monolayers need to be explored.

HCEC were originally believed to be incapable of expanding *in vitro*, but have been successfully isolated and cultured by introducing stimulating agents such as epidermal growth factor, platelet-derived growth factor-BB, bovine pituitary extract and fetal bovine serum [17,18]. However, the number of cells with proliferative activity and the ability to respond to such agents is relatively low, and much variation in proliferative activity exists between donors of different ages [19,20]. Thus, there is a requirement to achieve a stable and effective culture of cells in terms of both cell proliferation and physiologic function.

The HCEC cell cycle is mainly regulated by the p53 and pRB pathways, both of which have been inactivated by human papilloma virus (HPV) type 16 E6/E7 to successfully immortalize cells. Kim et al. reported the establishment of an immortalized HCEC line using HPV type 16 E6/E7 on lyophilized human amniotic membrane [21]. However, several studies have reported carcinogenesis of the cell line established by viral oncogenes including HPV type 16 E6/E7 or SV40 large T antigen [22,23]. Therefore a corneal endothelial cell line developed in this way does not appear to be suitable for the treatment of human corneal diseases. To resolve this problem, we expressed mutant cyclin-dependent kinase (Cdk) 4 and CyclinD1 to inactivate the pRB pathway and generate corneal endothelial cell lines without transducing viral oncogenes.

Results

HCEC with Descemet's membranes were proliferated slowly in a culture dish coated in type IV collagen. After two passages, the cells were transferred into 24-well dishes and transfected with a retroviral vector carrying E6/E7 or mutant Cdk4 and CyclinD1. Three cell lines were successfully generated, as shown in Fig. 1A, with obvious differences in growth (Fig. 1B). Protein expression from the transduced gene was confirmed by western blotting (Fig. 1C). As previously reported [21], THCEC (E6/E7) was immortalized, and THCEC (Cyclin) demonstrated the same proliferative capacity as THCEC (E6/E7), while primary cells grew more slowly even when cultured in 10% fetal bovine serum. These results indicate that induction of mutant Cdk4 and CyclinD1 is sufficient to generate a HCEC line that proliferates at a faster rate than the primary cell line.

Proliferation capacity was also confirmed by immunohistochemistry of Ki-67 (Fig. 2A). Expression of downstream genes of CyclinD1 which are associated with cell proliferation was analyzed by real-time polymerase chain reaction (PCR) (Fig. 2B). Positive staining of Ki-67, which is detected in the nucleus, was confirmed in both THCEC (Cyclin) and THCEC (E6/E7). Real-time PCR also revealed that CDC2 and PCNA, target genes of E2F (an upstream transcriptional factor), that are activated by CyclinD1, were up-regulated in THCEC (E6/E7) and especially in THCEC (Cyclin).

Expression of genes involved in active transmembrane transporter activity, including Na^+/K^+-ATPase, or cell adhesion, including ZO-1 and N-cadherin, were assessed by semi-quantitative reverse transcriptase (RT)-PCR (Fig. 3A). Expression of intercellular adhesion molecules was confirmed by immunohistochemistry (Fig. 3B–J). Semi-quantitative RT-PCR showed that there was no significant difference between the three cell lines regarding the expression of genes associated with several molecules of cell adhesion or of ion transporter channels, which are characteristically expressed by HCEC [21,24]. This was also confirmed by real-time PCR (data not shown).

ZO-1 and N-cadherin, key HCEC adhesion molecules [24], demonstrated positive staining at the intercellular junction in HCEH (Fig. 3F, I) and THCEC (Cyclin) (Fig. 3E, H), while neither ZO-1 nor N-cadherin was detected in THCEC (E6/E7) despite sufficient cellular density (Fig. 3G, J). Although positive staining of ZO-1 and N-cadherin was observed at the intercellular junction in THCEC (Cyclin), ZO-1 staining also occurred around the nucleus (Fig. 3E), indicating the immature distribution of the ZO-1 protein. In THCEC (Cyclin) and HCEC, hexagonal morphology was identified both by phase-contrast micrography (Fig. 3B, C) and immunocytochemistry, while the structure of hexagonal cell shape was not maintained in THCEC (E6/E7) (Fig. 3D). These data indicate that THCEC (Cyclin) and HCEC, but not THCEC (E6/E7), maintain contact inhibition which is crucial for preserving the monolayer.

Scanning electron microscopy was performed to reveal detailed information on the cellular junction (Fig. 4). THCEC (Cyclin) and HCEC showed a clear cellular junction including a tight junction, whereas THCEC (E6/E7) grew as a multilayer without forming a cellular junction, which confirms the immunohistochemistry result.

Representative traces of circuit current driven by the Na^+/K^+-ATPase were of similar shapes in both HCEC and THCEC (Cyclin) (Fig. 5A). These circuit currents maintain corneal translucency and their levels in both cell lines were clearly reduced by the presence of the Na^+/K^+-ATPase inhibitor ouabain, which confirms that the origin of the current is Na^+/K^+-ATPase. Meanwhile, the pump function in THCEC (Cyclin), detected in both earlier and later passages of cells, was more variable than that in HCEC (Fig. 5B), possibly indicating incomplete Na^+/K^+-ATPase activity or the presence of an intercellular barrier that regulates ion permeability. No regular circuit current was detected in THCEC (E6/E7) (Fig. 5A, B), which probably reflects the absence of intercellular adhesion preventing free ion transport across the membrane. This experiment clearly showed that the THCEC (Cyclin) monolayer has similar Na^+/K^+-ATPase activity to that of HCEC.

A tumorigenesis assay of nude mice detected no solid tumor in either THCEC (Cyclin) or THCEC (E6/E7), while HeLa cells formed a solid tumor in all mice (Table 1). Since THCEC (Cyclin) has a similar morphology and pump function to HCEC, THCEC (Cyclin) could be suitable for HCEC studies.

Discussion

THCEC (E6/E7) was shown to achieve immortalization with a highly activated proliferative capacity, as previously described [21]. However, the cell lines did not show normal intercellular contact or normal pump function, probably because contact inhibition in the cell line was not achieved. Meanwhile, THCEC (Cyclin) was demonstrated to have normal physiologic function with a greater proliferative capacity than primary cells, but slightly lower than that of THCEC (E6/E7).

In expanding the cellular life span, E7 has been shown to play a role in the inactivation of pRB, while E6 activates telomerase [25] and accelerates p53 degradation, which induces the Cdk inhibitor p21 [26]. However, little is known about the effector sites of the viral oncogene that may be related to genetic instability of immortalized cells. In the present study, expression of genes specific to HCEC was not drastically different between the three cell lines. However, key proteins including ZO-1 and N-cadherin that are important in forming intercellular contacts were detected, probably because of the unknown influence of viral oncogenes on post-translational modification, posttranslational import or protein stability/degradation.

We recently established genetically stable, non-transformed immortalized ovarian surface epithelium (OSE) cell lines without viral oncogenes by expressing mutant Cdk 4, CyclinD1 and hTERT, based on the hypothesis that inactivation of the pRb pathway and activation of telomerase are sufficient for OSE immortalization [27]. Meanwhile, Rane et al. demonstrated that mutant Cdk 4 (Cdk4R24C) is sufficient to induce carcinogenesis in several other tissues including those of the pancreas, pituitary and brain [28], and Joyce and colleagues showed that HCEC are arrested in the G1 phase and regulated by CKIs, p16INK4a and p21WAF1/Cip1 [29]. Considering the importance of maintaining

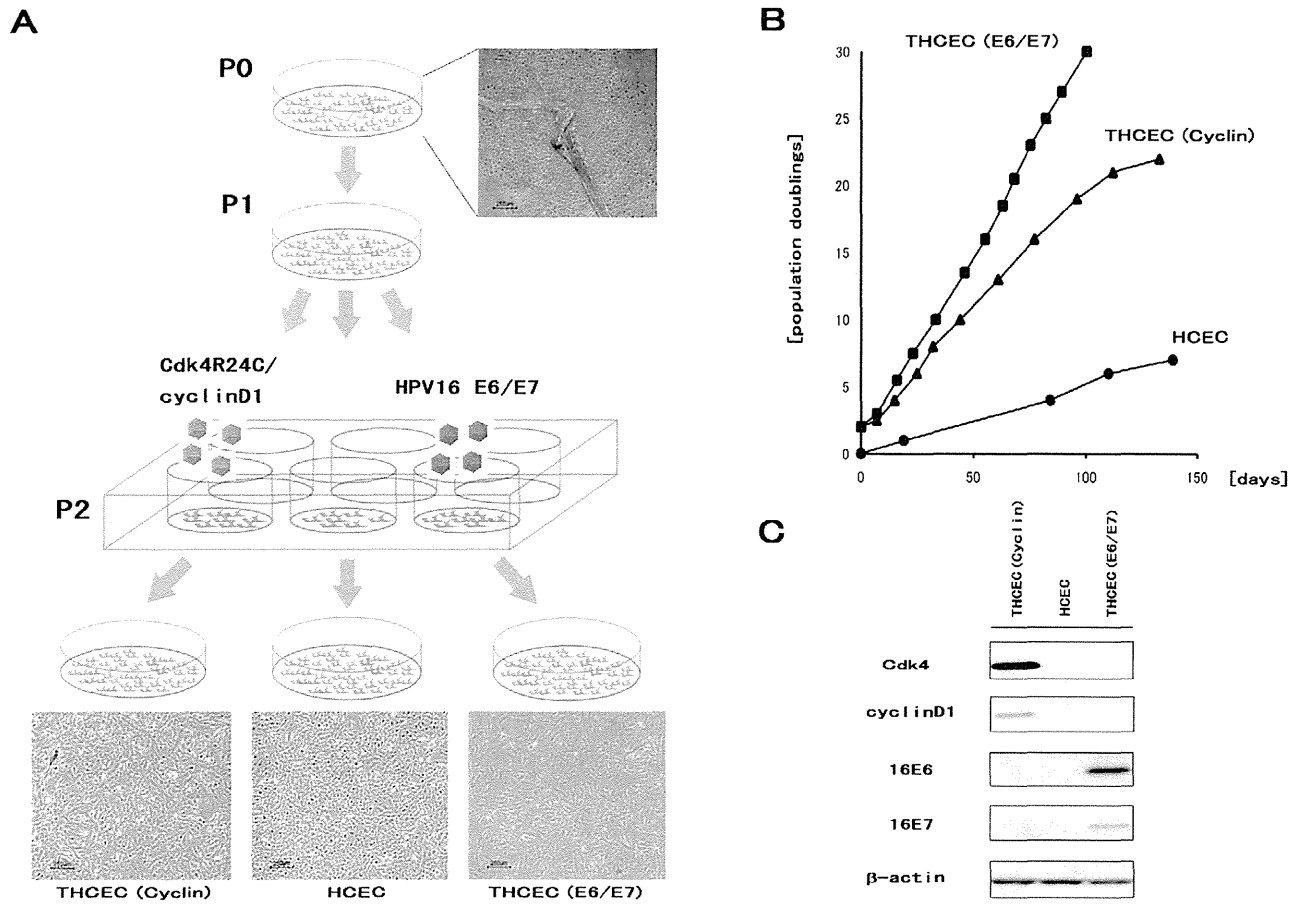

Figure 1. Establishment of THCEC (E6/E7), THCEC (Cyclin) and HCEC. (A) HCEC with Descemet's membrane were placed on Type IV collagen-coated 35 mm cell culture dishes with growth medium (P0). After one passage (P1), retroviral infection was conducted in 6-well cell culture dishes at P2. THCEC (E6/E7) and THCEC (Cyclin) were infected by retroviral vectors carrying HPV16 E6/E7 and both CyclinD1 and Cdk4R24C, respectively. (B) Growth curves of THCEC (E6/E7), THCEC (Cyclin) and HCEC cell lines. THCEC (E6/E7) was immortalized as reported previously, and THCEC (Cyclin) obtained the same proliferative activity as that of THCEC (E6/E7). Transfection was performed on day 0 for THCEC (E6/E7) and THCEC (Cyclin), with population doublings of 2. For HCEC, primary culture commenced on day 0. (C) Western blotting confirmed the expression of the following transgenes: E6 and E7 in THCEC (E6/E7), and CyclinD1 and Cdk4R24C in THCEC (Cyclin).
doi:10.1371/journal.pone.0029677.g001

morphology and physiologic function in HCEC, we only transduced mutant Cdk 4 and CyclinD1, not hTERT, in the present study. We believe that our careful method enabled THCEC (Cyclin) to form a fragile and regularly arranged monolayer complete with physiologic function.

Although THCEC (Cyclin) has similar characteristics to primary HCEC, immunohistochemistry and the Ussing chamber assay also highlighted the differences between the cells. ZO-1 protein was expressed around the nucleus of THCEC (Cyclin) but not in primary cells. Since semi-quantitative PCR detected almost the same level of mRNA expression between the cell lines, staining around the nucleus in THCEC (Cyclin) probably reflects an error in posttranslational import of ZO-1 protein. The Ussing chamber assay detected a similar pump function between THCEC (Cyclin) and primary cells, but the current in THCEC (Cyclin) was more variable than that of the primary cells, which might have been caused by reduced Na^+/K^+-ATPase activity, immature intercellular adhesion allowing irregular intercellular ion transport or differences in cellular density.

Cells established by a retrovirus carry a potential risk of promoting carcinogenesis [30], and direct transplantation to humans of cell sheets composed of such cells may lead to complex problems. Recently, to resolve this problem, several studies have reported the establishment of untransfected corneal endothelial cell lines [31,32,33], which are the most ideal cell lines for the treatment of human corneal disease. Meanwhile, alternative bioengineering approaches, including lipofection of p27kip1 siRNA [34], proteomics technology analyzing the difference between younger and older HCEC [35] and drug usage of promyelocytic leukemia zinc finger protein, a cell cycle transcriptional repressor and negative regulator [36], have also been introduced. The present findings support the idea that targeting the interaction between p16INK4a and Cdk4 using such methods is a promising strategy to generate HCEC with sufficient proliferative capacity and physiologic function.

Materials and Methods

Isolation and cell culture of human corneal cells

Ethics Statement. A cornea was excised from the surgically enucleated eye of a 2-year-old infant undergoing therapy for retinoblastoma, with the approval (approval number, #156) of the

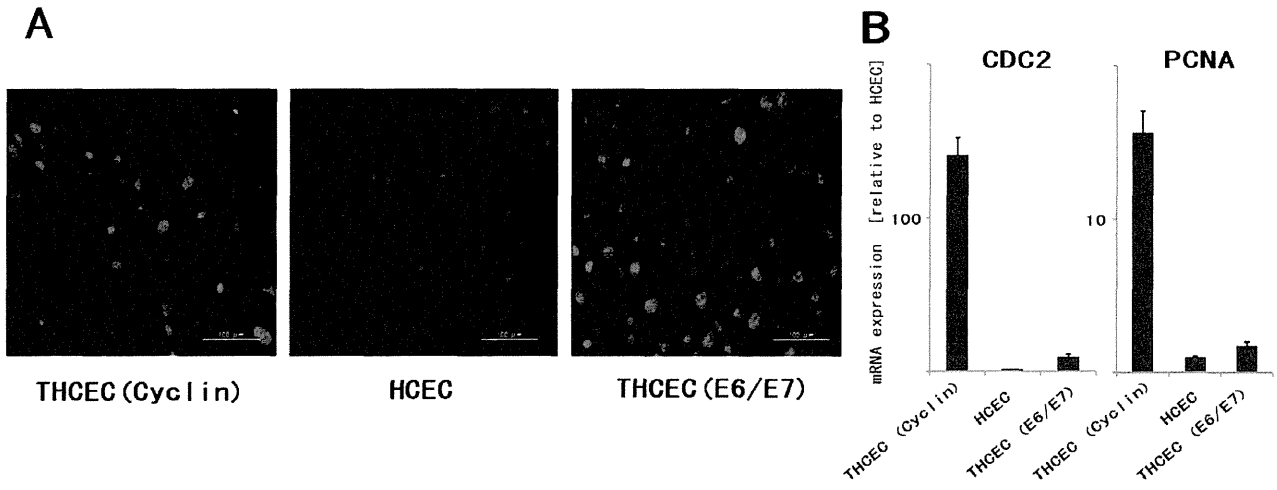

Figure 2. Evaluation of proliferative capacity. (A) Immunohistochemistry of Ki-67 in three cell lines. Positive staining of Ki-67, located in the nucleus, was obviously identified in THCEC (Cyclin) and THCEC (E6/E7), but rarely detected in HCEC. (B) Real-time PCR of downstream genes of cyclinD1 associated with proliferation. Gene expression levels of both CDC2 and PCAN were clearly higher than that of HCEC. The gene expression was much more activated in THCEC (Cyclin) in which the expression of E2F, an upstream transcriptional factor of two genes, was constitutively activated by transduced mutant Cdk4 and CyclinD1.
doi:10.1371/journal.pone.0029677.g002

Ethics Committee of the National Institute for Child and Health Development, Tokyo, Japan. Signed informed consent was obtained from the donor's parents, and the surgical specimens were irreversibly de-identified. All experiments handling human cells and tissues were performed in line with the tenets of the Declaration of Helsinki.

The corneal piece, which was grossly normal with no pathological lesions, was cut 1.5 mm from the corneal limbus,

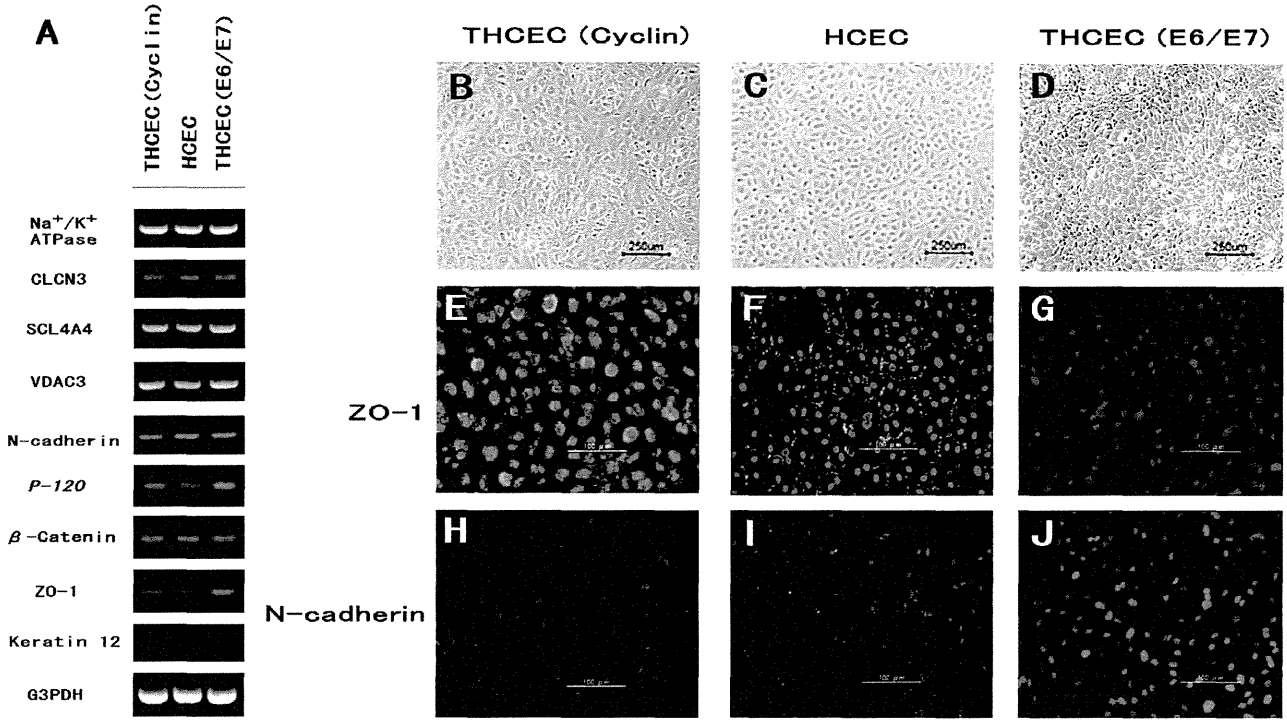

Figure 3. HCEC-associated genes and cytolocalization of junctional components expressed by cell lines. (A) Semi-quantitative reverse transcriptase polymerase chain reaction for HCEC-associated genes. Total RNA was prepared from cultured cells seven days after reaching confluency. No significant difference in mRNA expression was observed between the three cell lines. Compared with phase-contrast micrographs of (B) THCEC (Cyclin), (C) HCEC and (D) THCEC (E6/E7), cytolocalization was examined by immunofluorescence staining of ZO-1 (E, F,G) and N-cadherin (H, I, J). THCEC (E6/E7) did not stain positive for intercellular junctional molecules, while ZO-1 and N-cadherin stained positive at the junction in THCEC (Cyclin) and HCEC.
doi:10.1371/journal.pone.0029677.g003

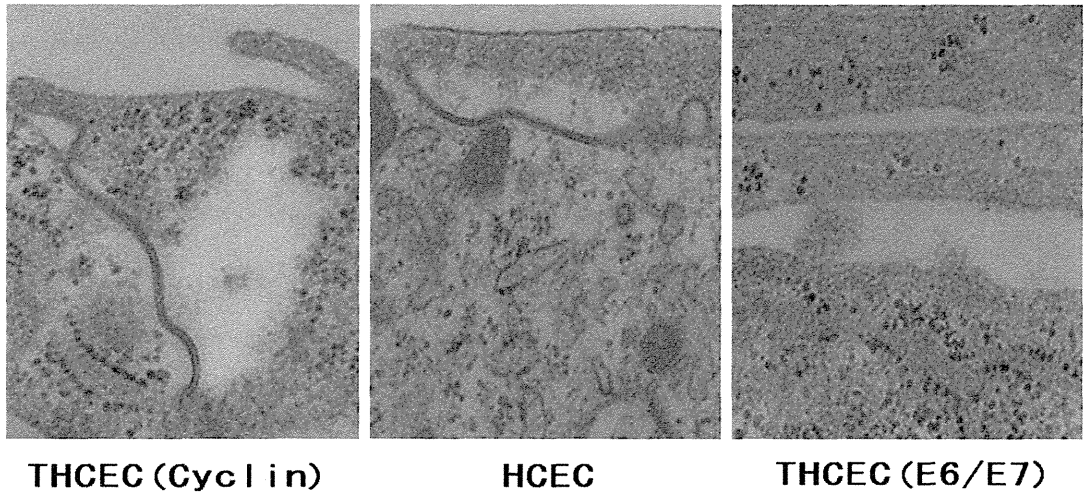

Figure 4. Transmission electron microscopy of cell line intercellular junctions. The junctional complex was detected at the intercellular junction in THCEC (Cyclin) and HCEC. No component of the intercellular junction was found in THCEC (E6/E7), in which cells grew in multilayers without being inhibited by cellular contact (scale bar = 200 nm).
doi:10.1371/journal.pone.0029677.g004

avoiding contamination of the trabecular meshwork tissue. HCEC with Descemet's membrane were stripped from the posterior surface of the corneal tissue with sterile surgical forceps under a dissecting microscope. They were cut into two pieces and cultured in a cell culture dish covered with Type IV collagen in a growth medium (GM); Dulbecco's modified Eagle's medium (DMEM)/Nutrient mixture F12 (1:1) with high glucose supplemented with 10% fetal bovine serum, insulin-transferrin-selenium and MEM-NEAA (Gibco, Auckland, NZ). Cells were subcultured after reaching confluency by treating with trypsin/EDTA and seeded at a density of 5×10^5 cells/well in 6-well dishes.

Viral vector construction and viral transduction

Lentiviral vector plasmids, CSII-CMV-cyclin D1 and -CDK4R24C were constructed by recombination using the Gateway system (Invitrogen, Carlsbad, CA) as described previously [37]. Briefly, cDNAs of human cyclinD1 and a mutant form of Cdk4 (Cdk4R24C: an inhibitor resistant form of Cdk4, generously provided by Dr Hara) were recombined with a lentiviral vector, CSII-CMV-RfA (a gift from Dr Miyoshi), by LR reaction to create a Gateway expression plasmid (Invitrogen) according to the manufacturer's instructions.

Previous work has described the production of recombinant lentiviruses with the vesicular stomatitis virus G glycoprotein [37], the recombinant retrovirus vector plasmid, pCLXSN-16E6E7 encoding HPV16 E6/E7 (16E6E7) [38] and recombinant retroviruses [39]. Following the addition of recombinant viral fluid to cells seeded in 24-well dishes in the presence of 4 μg/ml polybrene, the cells were infected by the viruses. Stably transduced cells with an expanded life span were designated transduced

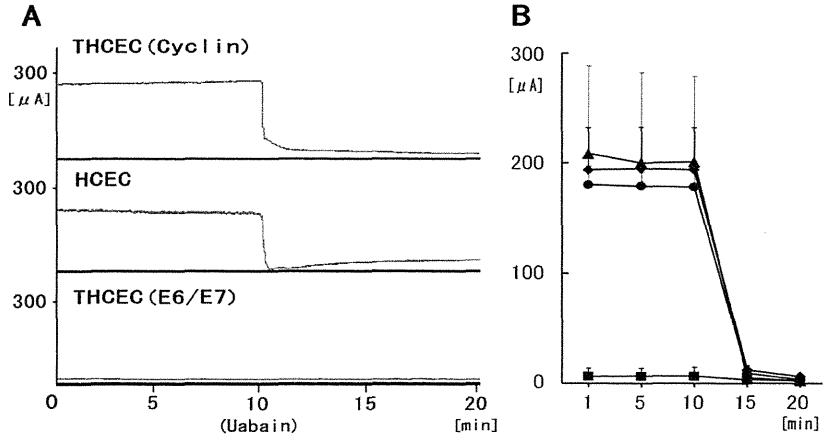

Figure 5. The pump function of cell lines. Short-circuit currents representing Na^+/K^+-ATPase activity from corneal cell monolayers on the insert well area of 4.67 cm^2 were calculated before and after addition of the Na^+/K^+-ATPase inhibitor ouabain. (A) Representative tracings of short-circuit current (μA/well) obtained with cell monolayers of THCEC (Cyclin) (upper panel), HCEC (middle panel) and THCEC (E6/E7) (lower panel). THCEC (Cyclin) possessed equal transport activity to HCEC, whereas no pump function was detected in THCEC (E6/E7). (B) Time-course changes in the average short circuit current of cultured monolayers of cell lines at 1, 5, 10 and 20 min. Data shown are for (▲) THCEC (Cyclin) at PD8, (♦) THCEC (Cyclin) at PD 21, (•) HCEC and (■) THCEC (E6/E7); all data are expressed as mean±SD of four replicate experiments of each cell line.
doi:10.1371/journal.pone.0029677.g005

Table 1. Tumorigenesis assay of cell lines in BALB/C nude mice.

Inoculated cells	Total dose (cell/mouse)	Number of mice (% mortality)	Number of mice with tumor
THCEC (Cyclin)	1.7×10^6	3(0)	0
THCEC (E6/E7)	1.7×10^6	3(0)	0
HeLa cells	2.0×10^6	3(0)	3

doi:10.1371/journal.pone.0029677.t001

human corneal endothelial cell by E6/E7 (THCEC (E6/E7)) and transduced human corneal endothelial cell by Cdk4R24C/cyclinD1 (THCEH (Cyclin)).

Culture of transfected cell lines and growth curve

When the cultures reached subconfluence, the cells were harvested with 0.25% trypsin and 1 mM EDTA, collected into tubes, and centrifuged. The cells were counted using a cell viability analyzer (Vi-CELL Cell Viability Analyzer, Beckman Coulter, Brea, CA), and population doubling (PD) was calculated. The pellets were suspended in growth medium, and the cells were passaged at a density of 5×10^5 cells/well in a 100-mm dish. The original cells were regarded as PD 2 (day 0).

Western blot analysis

Western blotting was conducted as described previously [40]. Antibodies against Cdk4 (ser473; Cell Signaling Technology, Danvers, MA), CyclinD1 (clone G124-326; BD Biosciences, Franklin Lakes, NJ), β-actin (sc-1616; Santa Cruz Biotechnology, Santa Cruz, CA) were used as probes, and horseradish peroxidase-conjugated anti-mouse, anti-rabbit (Jackson Immunoresearch Laboratories, West Grove, PA) or anti-goat (sc-2033; Santa Cruz Biotechnology, Santa Cruz, CA) immunoglobulins were employed as secondary antibodies.

Immunocytochemistry

Cell lines were grown on Type IV collagen-coated glass dishes 14 days after reaching confluency and were fixed with 4% formaldehyde (pH 7.0) for 15 min at room temperature. Cell lines were then rehydrated in phosphate buffered saline (PBS), incubated with 0.2% Triton X-100 for 15 min and rinsed three times with PBS for 5 min each. After incubation with 2% BSA to block nonspecific staining for 30 min, cell lines were incubated with anti-ZO-1 (1:50; sc-8146; Santa Cruz Biotechnology, Santa Cruz, CA), anti-N-cadherin (1:50; sc-7939; Santa Cruz Biotechnology) and anti-Ki67 (1:100; ab15580; Abcam, Cambridge, UK) for 16 h at 4°C. After three washes with PBS, cell lines were incubated with the secondary antibody for 60 min, followed by counterstaining with 4′,6-diamidino-2-phenylindole (1:200; sc-3598; Santa Cruz Biotechnology) for 10 min.

Semi-quantitative RT-PCR

Total RNA was extracted from 1×10^6 cultured HCEC using the RNeasy Plus mini-kitH (Qiagen, Germantown/Gaithersburg, MA) according to the manufacturer's instructions and quantified by absorption at 260 nm. Total RNA was then reverse-transcribed into cDNA using Superscript III Reverse Transcriptase (Invitrogen, Carlsbad, CA) with oligo random hexamers. cDNAs of each component were amplified by PCR using specific primers and DNA polymerase. The reaction was first incubated at 95°C for 10 min, followed by 39 cycles at 98°C for 30 s, 58°C for 30 s and 74°C for 30 s. PCR primers are listed in Table 2.

Quantitative real-time RT-PCR

Total RNA extraction and reverse transcription into cDNA was carried out as above. Each quantitative real-time RT-PCR for target genes, including Cell Division Cycle 2 (*CDC2*) and proliferating cell nuclear antigen (*PCNA*), was performed using the Chromo4 real time detection system (Bio-Rad, Hercules, CA). For a 20 ml PCR, the cDNA template was mixed with the primers to final concentrations of 200 nM and 10 µl of SsoFast EvaGreen Supermix (BIO-RAD), respectively. The reaction was first incubated at 95°C for 10 min, followed by 45 cycles at 95°C for 10 s, 57°C for 15 s, and 72°C for 20 s.

Transmission Electron Microscopy

Cell lines cultured on Type IV collagen-coated dishes were fixed in HEPES buffered 2% glutaraldehyde and subsequently post-fixed in 2% osmium tetroxide for 3 h on ice. Specimens were then dehydrated in graded ethanol and embedded in the epoxy resin. Ultrathin sections were obtained by ultramicrotomy and stained with uranyl acetate for 10 min and modified Sato's lead solution for 5 min then submitted to TEM observation (JEM-2000EX, JEOL).

Measurement of pump function

The pump function of confluent monolayers of HCEC was measured using an Ussing chamber as described previously [41]. Cells cultured on Snapwell inserts coated with Type IV collagen were placed in the Ussing chamber EM-CSYS-2 (Physiologic Instruments, San Diego, CA) with the endothelial cell surface side in contact with one chamber and the Snapwell membrane side in contact with another chamber. The chambers were carefully filled with Krebs-Ringer bicarbonate (120.7 mM NaCl, 24 mM $NaHCO_3$, 4.6 mM KCl, 0.5 mM $MgCl_2$, 0.7 mM Na_2HPO_4, 1.5 mM NaH_2PO_4 and 10 mM glucose bubbled with a mixture of 5% CO_2, 7% O_2 and 88% N_2 to pH 7.4). The chambers were maintained at 37°C using an attached heater.

The short-circuit current was sensed by narrow polyethylene tubes positioned close to either side of the Snapwell, filled with 3 M KCl and 4% agar gel and connected to silver electrodes. These electrodes were connected to the computer through the Ussing system VCC-MC2 (Physiologic Instruments) and an iWorx 118 Research Grade Recorder (iWorx Systems, Dover, NH), and the short-circuit current was recorded by Labscribe2 Software for Research (iWorx). After the short-circuit current had reached a steady state, ouabain (final concentration, 1 mM) was added to the chamber, and the short-circuit current was re-measured. The pump function attributable to Na^+/K^+-ATPase activity was calculated as the difference in short-circuit current measured before and after the addition of ouabain.

Tumorigenesis assay

Cells were harvested by Trypsin/EDTA treatment, collected into tubes, and centrifuged, and the pellets were suspended in

Table 2. Oligonucleotide sequences for RT-PCR.

Name	Sequence	Size (bp)	Accession Number
Collagen type IV	F: 5′-GGC ACC TGC CAC TAC TAC GC-3′	472	NM_001845
	R: 5′-TCA CCA GGA GGT AGC CGA T-3′		
Keratin 12	F: 5′-GAT GCT AAT GCT GAG CTC GA-3′	393	NM_000223
	R: 5′-ACC TGC CCT ACA GCT TTG TA-3		
VDAC3	F: 5′-TGA CTC TTG ATA CCA TAT TTG TAC CG-3′	482	NM_001135694
	R: 5′-TCA ATT TGA CTC CTG GTC GAA-3′		
CLCN3	F: 5′-AGA AAG GCA TAG ACG GAT CAA-3′	204	NM_001829
	R: 5′-GGT TGT ACC ACA ACG CAC TAA-3′		
SLC4A4	F: 5′-GTT CAG ATG AAT GGG GAT ACGC	697	NM_001136260
	R: 5′-CGA GCA TAA ACA CAA AGC GTA A-3′		
Na^+/K^+-ATPase	F: 5′-CCC AGG ACT CAT GGT TTT TC-3′	482	NM_000702
	R: 5′-GGA GCA AAG CTG ACC TGA AC-3′		
N-cadherin	F: 5′-CAA CTT GCC AGA AAA CTC CAG G-3′	205	NM_ 001792
	R: 5′-ATG AAA CCG GGC TAT CTG CTC-3′		
β-catenin	F: 5′-TAC CTC CCA AGT CCT GTA TGA G-3′	180	NM _001904
	R: 5′-TGA GCA GCA TCA AAC TGT GTA G-3′		
P-120	F: 5′-CCC CAG GAT CAC AGT CAC CT-3′	144	NM_001085467
	R: 5′-CCG AGT GGT CCC ATC ATC TG-3′		
ZO-1	F: 5′-AGT CCC TTA CCT TTC GCC TGA-3′	180	NM_003257
	R: 5′-TCT CTT AGC ATT ATG TGA GCT GC-3′		
GAPDH	F: 5′-GCT CAG ACA CCA TGG GGA AGG T-3′	474	NM_002046
	R: 5′-GTG GTG CAG GAG GCA TTG CTG A-3′		
PCNA	F: 5′- GCGTGAACCTCACCAGTATGT-3′	76	NM_002592
	R: 5′- TCTTCGGCCCTTAGTGTAATGAT-3′		
CDC2	F: 5′- GGATGTGCTTATGCAGGATTCC-3′	100	NM_001786
	R: 5′- CATGTACTGACCAGGAGGGATAG-3′		

VDAC3: voltage-dependent anion channel 3, CLCN3: chloride channel protein 3, SLC4A4: sodium bicarbonate cotransporter membrane.
doi:10.1371/journal.pone.0029677.t002

DMEM. The same volume of Basement Membrane Matrix (BD Biosciences) was added to the cell suspension. Cells (1.7×10^6) of THCEC (Cyclin) and THCEC (E6/E7) were inoculated subcutaneously into dorsal flanks of each of three Balb/c nu/nu mice (CREA, Japan) for 60 days. A total of 2.0×10^6 HeLa cells per mouse were used as positive controls. The skin of dorsal flanks of inoculated mice was surgically opened and the tumorigenic status was examined.

Author Contributions

Conceived and designed the experiments: Tadashi Yokoi YS Tae Yokoi TK AU HN NA. Performed the experiments: Tadashi Yokoi YS Tae Yokoi HM SH MY TK HN NA. Analyzed the data: Tadashi Yokoi YS Tae Yokoi HM SH MY AU HN NA. Contributed reagents/materials/analysis tools: Tadashi Yokoi SH MY TK HN NA. Wrote the paper: Tadashi Yokoi YS TK AU HN NA.

References

1. Hatou S, Yamada M, Mochizuki H, Shiraishi A, Joko T, et al. (2009) The effects of dexamethasone on the Na,K-ATPase activity and pump function of corneal endothelial cells. Curr Eye Res 34: 347–354.
2. Barfort P, Maurice D (1974) Electrical potential and fluid transport across the corneal endothelium. Exp Eye Res 19: 11–19.
3. Bourne WM, Nelson LR, Hodge DO (1997) Central corneal endothelial cell changes over a ten-year period. Invest Ophthalmol Vis Sci 38: 779–782.
4. Hashemian MN, Moghimi S, Fard MA, Fallah MR, Mansouri MR (2006) Corneal endothelial cell density and morphology in normal Iranian eyes. BMC Ophthalmol 6: 9.
5. Padilla MD, Sibayan SA, Gonzales CS (2004) Corneal endothelial cell density and morphology in normal Filipino eyes. Cornea 23: 129–135.
6. Adamis AP, Filatov V, Tripathi BJ, Tripathi RC (1993) Fuchs' endothelial dystrophy of the cornea. Surv Ophthalmol 38: 149–168.
7. Schultz RO, Matsuda M, Yee RW, Edelhauser HF, Schultz KJ (1984) Corneal endothelial changes in type I and type II diabetes mellitus. Am J Ophthalmol 98: 401–410.
8. Slingsby JG, Forstot SL (1981) Effect of blunt trauma on the corneal endothelium. Arch Ophthalmol 99: 1041–1043.
9. Bourne WM, Nelson LR, Hodge DO (1994) Continued endothelial cell loss ten years after lens implantation. Ophthalmology 101: 1014–1022;discussion 1022–1013.
10. Gagnon MM, Boisjoly HM, Brunette I, Charest M, Amyot M (1997) Corneal endothelial cell density in glaucoma. Cornea 16: 314–318.
11. Laing RA, Sanstrom MM, Berrospi AR, Leibowitz HM (1976) Changes in the corneal endothelium as a function of age. Exp Eye Res 22: 587–594.
12. Landshman N, Ben-Hanan I, Assia E, Ben-Chaim O, Belkin M (1988) Relationship between morphology and functional ability of regenerated corneal endothelium. Invest Ophthalmol Vis Sci 29: 1100–1109.
13. Coster DJ, Williams KA (2005) The impact of corneal allograft rejection on the long-term outcome of corneal transplantation. Am J Ophthalmol 140: 1112–1122.
14. Terry MA, Ousley PJ (2001) Deep lamellar endothelial keratoplasty in the first United States patients: early clinical results. Cornea 20: 239–243.
15. Price FW Jr., Price MO (2005) Descemet's stripping with endothelial keratoplasty in 50 eyes: a refractive neutral corneal transplant. J Refract Surg 21: 339–345.
16. Melles GR, Ong TS, Ververs B, van der Wees J (2006) Descemet membrane endothelial keratoplasty (DMEK). Cornea 25: 987–990.

17. Zhu C, Joyce NC (2004) Proliferative response of corneal endothelial cells from young and older donors. Invest Ophthalmol Vis Sci 45: 1743–1751.
18. Li W, Sabater AL, Chen YT, Hayashida Y, Chen SY, et al. (2007) A novel method of isolation, preservation, and expansion of human corneal endothelial cells. Invest Ophthalmol Vis Sci 48: 614–620.
19. Ishino Y, Zhu C, Harris DL, Joyce NC (2008) Protein tyrosine phosphatase-1B (PTP1B) helps regulate EGF-induced stimulation of S-phase entry in human corneal endothelial cells. Mol Vis 14: 61–70.
20. Senoo T, Joyce NC (2000) Cell cycle kinetics in corneal endothelium from old and young donors. Invest Ophthalmol Vis Sci 41: 660–667.
21. Kim HJ, Ryu YH, Ahn JI, Park JK, Kim JC (2006) Characterization of immortalized human corneal endothelial cell line using HPV 16 E6/E7 on lyophilized human amniotic membrane. Korean J Ophthalmol 20: 47–54.
22. Nitta M, Katabuchi H, Ohtake H, Tashiro H, Yamaizumi M, et al. (2001) Characterization and tumorigenicity of human ovarian surface epithelial cells immortalized by SV40 large T antigen. Gynecol Oncol 81: 10–17.
23. Tsao SW, Mok SC, Fey EG, Fletcher JA, Wan TS, et al. (1995) Characterization of human ovarian surface epithelial cells immortalized by human papilloma viral oncogenes (HPV-E6E7 ORFs). Exp Cell Res 218: 499–507.
24. Zhu YT, Hayashida Y, Kheirkhah A, He H, Chen SY, et al. (2008) Characterization and comparison of intercellular adherent junctions expressed by human corneal endothelial cells in vivo and in vitro. Invest Ophthalmol Vis Sci 49: 3879–3886.
25. Kiyono T, Foster SA, Koop JI, McDougall JK, Galloway DA, et al. (1998) Both Rb/p16INK4a inactivation and telomerase activity are required to immortalize human epithelial cells. Nature 396: 84–88.
26. Sekiguchi T, Hunter T (1998) Induction of growth arrest and cell death by overexpression of the cyclin-Cdk inhibitor p21 in hamster BHK21 cells. Oncogene 16: 369–380.
27. Sasaki R, Narisawa-Saito M, Yugawa T, Fujita M, Tashiro H, et al. (2009) Oncogenic transformation of human ovarian surface epithelial cells with defined cellular oncogenes. Carcinogenesis 30: 423–431.
28. Rane SG, Cosenza SC, Mettus RV, Reddy EP (2002) Germ line transmission of the Cdk4(R24C) mutation facilitates tumorigenesis and escape from cellular senescence. Mol Cell Biol 22: 644–656.
29. Enomoto K, Mimura T, Harris DL, Joyce NC (2006) Age differences in cyclin-dependent kinase inhibitor expression and rb hyperphosphorylation in human corneal endothelial cells. Invest Ophthalmol Vis Sci 47: 4330–4340.
30. Robinson HL (1982) Retroviruses and cancer. Rev Infect Dis 4: 1015–1025.
31. Fan T, Zhao J, Ma X, Xu X, Zhao W, et al. (2011) Establishment of a continuous untransfected human corneal endothelial cell line and its biocompatibility to denuded amniotic membrane. Mol Vis 17: 469–480.
32. Fan T, Wang D, Zhao J, Wang J, Fu Y, et al. (2009) Establishment and characterization of a novel untransfected corneal endothelial cell line from New Zealand white rabbits. Mol Vis 15: 1070–1078.
33. Valtink M, Gruschwitz R, Funk RH, Engelmann K (2008) Two clonal cell lines of immortalized human corneal endothelial cells show either differentiated or precursor cell characteristics. Cells Tissues Organs 187: 286–294.
34. Kikuchi M, Zhu C, Senoo T, Obara Y, Joyce NC (2006) p27kip1 siRNA induces proliferation in corneal endothelial cells from young but not older donors. Invest Ophthalmol Vis Sci 47: 4803–4809.
35. Zhu C, Rawe I, Joyce NC (2008) Differential protein expression in human corneal endothelial cells cultured from young and older donors. Mol Vis 14: 1805–1814.
36. Shiraishi A, Joko T, Higashiyama S, Ohashi Y (2007) Role of promyelocytic leukemia zinc finger protein in proliferation of cultured human corneal endothelial cells. Cornea 26: S55–58.
37. Miyoshi H, Blomer U, Takahashi M, Gage FH, Verma IM (1998) Development of a self-inactivating lentivirus vector. J Virol 72: 8150–8157.
38. Narisawa-Saito M, Yoshimatsu Y, Ohno S, Yugawa T, Egawa N, et al. (2008) An in vitro multistep carcinogenesis model for human cervical cancer. Cancer Res 68: 5699–5705.
39. Naviaux RK, Costanzi E, Haas M, Verma IM (1996) The pCL vector system: rapid production of helper-free, high-titer, recombinant retroviruses. J Virol 70: 5701–5705.
40. Haga K, Ohno S, Yugawa T, Narisawa-Saito M, Fujita M, et al. (2007) Efficient immortalization of primary human cells by p16INK4a-specific short hairpin RNA or Bmi-1, combined with introduction of hTERT. Cancer Sci 98: 147–154.
41. Mimura T, Yamagami S, Yokoo S, Usui T, Tanaka K, et al. (2004) Cultured human corneal endothelial cell transplantation with a collagen sheet in a rabbit model. Invest Ophthalmol Vis Sci 45: 2992–2997.

STEM CELLS AND DEVELOPMENT
Volume 21, Number 7, 2012

DOI: 10.1089/scd.2011.0229

Prospective Isolation and Characterization of Bipotent Progenitor Cells in Early Mouse Liver Development

Ken Okada,[1,2] Akihide Kamiya,[1] Keiichi Ito,[1] Ayaka Yanagida,[1] Hidenori Ito,[1] Hiroki Kondou,[3] Hiroshi Nishina,[4] and Hiromitsu Nakauchi[1,5]

Outgrowth of the foregut endoderm to form the liver bud is considered the initial event of liver development. Hepatic stem/progenitor cells (HSPCs) in the liver bud are postulated to migrate into septum transversum mesenchyme at around embryonic day (E) 9 in mice. The studies of liver development focused on the mid-fetal stage (E11.5–14.5) have identified HSPCs at this stage. However, the in vitro characteristics of HSPCs before E11.5 have not been elucidated. This is probably partly because purification and characterization of HSPCs in early fetal livers have not been fully established. To permit detailed phenotypic analyses of early fetal HSPC candidates, we developed a new coculture system, using mouse embryonic fibroblast cells. In this coculture system, $CD13^+Dlk^+$ cells purified from mouse early fetal livers (E9.5 and E10.5) formed colonies composed of both albumin-positive hepatocytic cells and cytokeratin (CK) 19-positive cholangiocytic cells, indicating that early fetal $CD13^+Dlk^+$ cells have properties of bipotent progenitor cells. Inhibition of signaling by Rho-associated coiled-coil containing protein kinase (Rock) or by nonmuscle myosin II (downstream from Rock) was necessary for effective expansion of early fetal $CD13^+Dlk^+$ cells in vitro. In sorted $CD13^+Dlk^+$ cells, expression of the hepatocyte marker genes albumin and α-fetoprotein increased with fetal liver age, whereas expression of CK19 and Sox17, endodermal progenitor cell markers, was highest at E9.5 but decreased dramatically thereafter. These first prospective studies of early fetal HSPC candidates demonstrate that bipotent stem/progenitor cells exist before E11.5 and implicate Rock-myosin II signaling in their development.

Introduction

Liver development is regulated by hormonal factors as well as by cell–cell interaction. In the beginning of liver development, around embryonic day (E) 9 in mice, hepatic stem/progenitor cells (HSPCs) are believed to differentiate from foregut endoderm and to expand in the early fetal liver bud. Fibroblast growth factor derived from the cardiac mesoderm and bone-morphogenetic proteins from septum transversum mesenchyme are important for differentiation of foregut endodermal cells into hepatic-lineage cells [1,2]. During mid- to late-fetal development (around E11.5 to E16.5), hematopoietic stem cells originating from the aorta-gonad-mesonephros region migrate into the fetal liver. This implies significant change in the microenvironment of the liver from early- to late-fetal liver development. Oncostatin M secreted from hematopoietic cells induces hepatoblasts, hepatic progenitor cells in mid-fetal livers, to differentiate into mature hepatocytes [3,4]. Hepatoblasts can proliferate at high rate and possess bipotency, the ability to differentiate into both hepatocytes (hepatic parenchymal cells) and cholangiocytes [5]. Several groups have purified hepatoblasts derived from E11.5 to E14.5 livers. We have shown that a sorted individual cell derived from mid-fetal liver gives rise to a relatively large colony after 5 days of culture on extracellular matrix-coated dishes [6]. A member of this class of cells is designated as a "hepatic colony-forming unit in culture (H-CFU-C)." Utilizing H-CFU-C culture, delta-like 1 homolog (Dlk), Liv2, CD13, and CD133 were identified as cell surface markers for hepatoblasts [7–9]. H-CFU-C culture and reclone sorting have demonstrated that hepatoblasts in mid-fetal livers have self-renewal capacity and bipotency [10]. Several transcription factors, such as Prox1, Tbx3, and Sall4, regulate proliferation and differentiation of hepatoblasts in liver development [11–13].

[1]Division of Stem Cell Therapy, Center for Stem Cell Biology and Regenerative Medicine, The Institute of Medical Science, The University of Tokyo, Tokyo, Japan.
[2]Core Research for Evolutional Science and Technology, Japan Science and Technology Agency, Saitama, Japan.
[3]Department of Pediatrics, Graduate School of Medicine, Osaka University, Osaka, Japan.
[4]Department of Developmental and Regenerative Biology, Medical Research Institute, Tokyo Medical and Dental University, Tokyo, Japan.
[5]Exploratory Research for Advanced Technology, Japan Science and Technology Agency, Saitama, Japan.

In contrast to hepatoblasts in mid-fetal livers, few studies have been done with early fetal HSPCs in E9.5 and 10.5 liver buds (Fig. 1A), because no suitable culture system for these cells has been established. HSPCs in early fetal livers thus remain largely uncharacterized. Explant culture systems have been used to study early fetal liver cells, and the effects of fibroblast growth factor secreted from cardiac mesoderm on early fetal livers were found using explanted-liver organ culture [1,2]. However, as explanted early fetal livers do not consist solely of HSPCs, to establish a culture system for purified progenitor cells in such livers is crucial for analyses of the initial steps of liver development. In this study, we found that cells expressing CD13, Dlk, and Liv2 exist during early- to mid-fetal liver development. We established a new culture system for in vitro expansion of these cells, candidate HSPCs, at the single-cell level using mouse embryonic fibroblasts (MEFs) as feeder cells. $CD13^+Dlk^+$ cells derived from early fetal liver showed bipotency and could proliferate to form large colonies in this culture system. Inhibition of Rho-associated coiled-coil–containing protein kinase (Rock) or myosin II activity using, respectively, Y-27632 or blebbistatin significantly enhanced colony-forming activities of early fetal $CD13^+Dlk^+$ cells. This study, the first investigation of purified HSPCs derived from early fetal livers, demonstrates that these progenitor cells in early fetal livers have properties distinct from those in mid-fetal livers.

Materials and Methods

Materials

C57BL/6NCrSlc, C3H, and green fluorescent protein (GFP)-transgenic mice (Nihon SLC, Shizuoka, Japan) were used in this study. All animals were treated under guidelines of the Institute of Medical Science, The University of Tokyo. Reagents and commercial suppliers were Dulbecco's modified Eagle's medium (DMEM), DMEM/Ham's F12 half medium, penicillin/streptomycin/L-glutamine (100×), dexamethasone, dimethyl sulfoxide, nicotinamide, and gelatin from porcine skin (Sigma, St. Louis, MO); insulin–transferrin–selenium X, nonessential amino acid solution, KnockOut Serum Replacement (KSR), and HEPES buffer solution (Invitrogen, Carlsbad, CA); fetal bovine serum (FBS; Nichirei Biosciences, Tokyo, Japan); hepatocyte growth factor and epidermal growth factor (PeproTech, Rocky Hill, NJ); collagen type I (Nitta Gelatin, Osaka, Japan); PD0325901 and CHIR99021 (Axon Biochemicals, Groningen, The Netherlands); Y-27632 (Wako Pure Chemical Industries, Osaka, Japan); A-83-01 (Tocris Bioscience, Bristol, United Kingdom); and (S)-(−)-blebbistatin (Toronto Research Chemicals, Inc., Toronto, ON). Phycoerythrin (PE)-conjugated anti-CD13 (Pharmingen, San Jose, CA), fluorescein isothiocyanate (FITC)-conjugated anti-Dlk (Medical and Biological Laboratories, Nagoya, Japan), allophycocyanin (APC)-conjugated

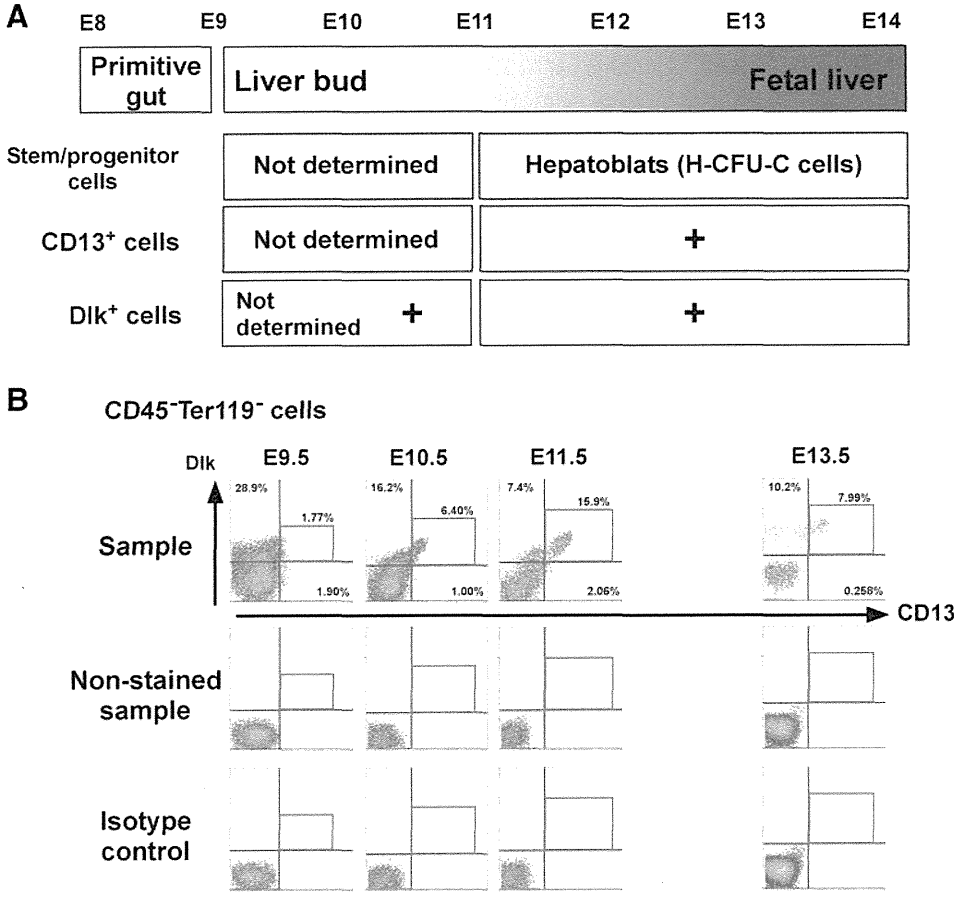

FIG. 1. Expression of cell surface markers in early- to mid-fetal liver cells. **(A)** Studies of hepatic stem/progenitor cells (HSPCs) during embryonic development. Bipotent progenitor cells in E11–14 mid-fetal livers (hepatoblasts) have been well characterized using H-CFU-C assays. In contrast, progenitor cells in early fetal livers (E9–10) have not been previously purified. **(B)** Cells from E9.5, E10.5, E11.5, and E13.5 fetal livers were stained with antibodies to various markers against mid-fetal hepatoblasts (CD13 and Dlk) and hematopoietic cells (CD45 and Ter119). Some populations of $CD45^-Ter119^-$ nonhematopoietic cells in early- and mid-fetal livers expressed both CD13 and Dlk. Nonstained cells (Nonstained sample), cells stained with isotype antibodies (Isotype control), or cells stained with anti-mouse CD13 and Dlk antibodies (Sample) were analyzed using flow cytometer. Ratios of CD13-single positive, Dlk-single positive, and $CD13^+Dlk^+$ cells in the $CD45^-Ter119^-$ fraction are shown. Numbers of $CD13^+Dlk^+$ cells in each of the $CD45^-Ter119^-$ fractions are as follows: 652 in 36,796 (E9.5), 1,630 in 25,481 (E10.5), 2,764 in 17,429 (E11.5), and 526 in 6,587 (E13.5). H-CFU-C, hepatic colony-forming unit in culture.

anti-Ter119, and APC-conjugated anti-CD45.2 (eBioscience, San Diego, CA) antibodies were used for cell staining.

Flow cytometric analysis

Minced liver tissues from E9.5 through E13.5 mice were dissociated with 0.05% collagenase solution. Dissociated cells were washed with phosphate-buffered saline (PBS) supplemented with 3% FBS and incubated with antibodies against cell surface markers for 60 min at 4°C. After washing with PBS supplemented with 3% FBS and staining of dead cells with propidium iodide, the cells were analyzed and sorted using a MoFlo™ fluorescence-activated cell sorter (DAKO, Glostrup, Denmark). Results with isotype control antibodies were shown as negative control.

Analysis of Liv2 expression using a fluorescence-activated flow cytometer

Dissociated cells were incubated with rat anti-Liv2 antibody [8] for 30 min on ice. After washing with PBS supplemented with 3% FBS, cells were stained with anti-rat immunoglobulin G (IgG)-Alexa647 (Invitrogen) for 30 min on ice and were washed with PBS supplemented with 3% FBS. Cells were further stained with FITC-conjugated anti-Dlk, PE-conjugated anti-CD13, PE-Cy7-conjugated anti-CD45, and PE-Cy7-conjugated anti-Ter119 (eBioscience) antibodies for 30 min on ice. After washing with PBS supplemented with 3% FBS and staining of dead cells with propidium iodide, the cells were analyzed and sorted using a MoFlo fluorescence-activated cell sorter.

Preparation of MEF

E13.5 ICR mouse embryos (Nihon SLC) were dissected and the head and internal organs were completely removed. The torso was minced and dissociated in 0.05% trypsin–EDTA (Sigma) for 30 min. After washing with PBS, cells were expanded in DMEM with 10% FBS. To halt cell proliferation, these MEFs were treated with mitomycin C (Wako Pure Chemical Industries) at 37°C for 2 h and used as feeder cells.

Colony formation assay

$CD13^+Dlk^+$ and other types of cells in the nonhematopoietic cell fraction were plated onto type I collagen or gelatin-coated 35-mm tissue culture dishes at a low density (25 cells/cm^2) or into type I collagen-coated 96-well plates at one cell per well. For colony formation assay with feeder cells, mitomycin C-treated feeder cells (MEF or other cell lines) were plated onto 0.1% gelatin-coated 12-well plates (2×10^5 cells per well). After 24 h of culture, cells in the nonhematopoietic cell fraction were sorted onto feeder cells at a low density (25 cells/cm^2).

Our standard culture medium is a 1:1 mixture of H-CFU-C medium (DMEM/Ham's F12 half medium with 10% FBS or 10% KSR, 1× Insulin–Transferrin–Selenium X, 10 mM nicotinamide, 10^{-7} M dexamethasone, 2.5 mM HEPES, 1× penicillin/streptomycin/L-glutamine, and 1× nonessential amino acid solution) and conditioned medium derived from E14.5 hepatic cells [13]. In several experiments, we used a 1:1 mixture of H-CFU-C medium and fresh DMEM with 10% KSR as a culture medium for coculture colony assays. Cells were cultured for 6 days, in the presence of 40 ng/mL hepatocyte growth factor and 20 ng/mL epidermal growth factor, in either standard culture medium or 1:1 mixture of H-CFU-C medium and fresh DMEM with 10% KSR. To count colonies derived from individual single cells, we used an ArrayScan VTI HCS Reader (Thermo Scientific, Waltham, MA) following immunostaining. Albumin-positive colonies were counted.

To analyze the effects of Rock-myosin II pathway using inhibitors, $CD45^-Ter119^-Dlk^+$ cells derived from GFP transgenic mouse embryos were cocultured with MEF in the presence of either Y-27632 or blebbistatin. GFP-positive colonies were counted. To analyze the effects of soluble factors derived from MEF, MEF-conditioned medium was harvested from 2-day confluent cultures of MEF cultured in a 1:1 mixture of H-CFU-C medium and fresh DMEM with 10% KSR. We cultured early fetal cells on collagen-coated dishes or on MEF feeder cells in MEF-conditioned medium.

Messenger RNA detection by reverse transcription–polymerase chain reaction

Total RNA was extracted from $CD13^+Dlk^+$ cells in the nonhematopoietic cell fraction using the RNeasy Micro Kit (Qiagen, Venlo, The Netherlands). First-strand cDNA synthesized using the Primescript first strand cDNA synthesis kit (Takara, Otsu, Japan) was used as a template for quantitative reverse transcription–polymerase chain reaction (RT-PCR) amplification. The cDNA samples were normalized by number of glyceraldehyde 3-phosphate dehydrogenase copies using quantitative RT-PCR with the TaqMan probe (Applied Biosystems, Foster City, CA). Universal Library (Roche Diagnosis, Basel, Switzerland) was used to quantify the copy numbers of albumin, α-fetoprotein (AFP), cytokeratin (CK) 19, c-Met, E-cadherin, and Sox17 transcripts. Intron-spanning primer sequences and probe number for each gene are shown in Supplementary Table S1 (Supplementary Data are available online at www.liebertonline.com/scd).

For hepatic gene expression analyses in HSPC colonies, E10.5 and E13.5 $CD13^+Dlk^+$ cells derived from GFP-transgenic mice were cultured with MEF for 3 days. Colonies were dissociated in 0.05% trypsin–EDTA and GFP^+ cells were purified using a MoFlo fluorescence-activated cell sorter. Total RNA was extracted and first-strand cDNA was synthesized using High-Capacity cDNA Reverse Transcription Kit (Applied Biosystems). Expression of hepatic genes was detected using quantitative RT-PCR with the TaqMan probe: Cyp1A1, Mm00487218_m1; Cyp1A2, Mm00487224_m1; Cyp3A11, Mm00731567_m1; Cyp3A13, Mm00484110_m1; Cyp7a1, Mm00484152_m1; glucose-6-phosphatase, Mm00839363_m1; tyrosine aminotransferase, Mm01244282_m1; albumin, Mm00802090_m1; CK19, Mm00492980_m1.

Immunostaining

Cultured cells were washed with PBS and were fixed with 4% paraformaldehyde/PBS. After washing 3 times with PBS, cells were permeabilized with 0.5% Triton/PBS for 10 min, washed with PBS, and incubated with 5% donkey serum/PBS for 1 h at room temperature. They were incubated with diluted primary antibodies overnight at 4°C. Goat anti-albumin antibody (Bethyl, Montgomery, TX) and rabbit anti-CK19 antibody (A gift from Prof. A. Miyajima, University of

Tokyo, Tokyo, Japan) were used as primary antibodies [7]. The cells next were washed with PBS and were incubated for 1 h at room temperature with anti-rabbit IgG-Alexa488 and anti-goat IgG-Alexa546 antibodies (Invitrogen). The cells were washed with PBS and their nuclei were stained with 40,6-diamidine-20-phenylindole dihydrochloride (Sigma).

For the analyses of proliferation, colonies were stained with goat anti-albumin antibody and rabbit anti-Ki67 antibody (Abcam, Cambridge, United Kingdom). After washing with PBS, cells were stained with anti-rabbit IgG-Alexa555 and anti-goat IgG-Alexa488 antibodies (Invitrogen). Intensities of Ki67 in individual albumin-positive colonies were analyzed with an ArrayScan VTI HCS Reader.

In-droplet cell-staining methods

To quantify albumin and CK19 expression in individual cells, in-droplet staining methods were used [14]. $CD13^+Dlk^+$ cells derived from fetal livers were sorted onto slide glasses. After fixation with 2% paraformaldehyde/PBS and permeabilization with 0.5% Triton/PBS, cells were incubated in 5% donkey serum/PBS for 30 min at room temperature. They then were incubated with goat anti-albumin and rabbit anti-CK19 antibodies overnight at 4°C, washed with PBS, and incubated with secondary antibodies (anti-rabbit IgG-Alexa488 and anti-goat IgG-Alexa546 antibodies) for 40 min at room temperature. The cells were washed with PBS and their nuclei were stained with 40,6-diamidine-20-phenylindole dihydrochloride. For each analysis, addition of an appropriate immune serum provided a negative control. Antibody fluorescence intensity was measured using the ArrayScan Reader.

Statistics

We used Microsoft Excel 2004 for Mac, Version 11.6.2 (Microsoft, Redmond, WA) to calculate standard deviations (SDs) and statistically significant differences between samples using Student's 2-tailed *t*-test.

Results

Early fetal liver contains cells expressing mid-fetal hepatoblast cell-surface markers

Several studies show that CD13 and Dlk are cell surface markers of hepatoblasts in mid-fetal livers (E11.5 to E14.5) and hepatoblasts exist in the $CD13^+Dlk^+$ fraction [7,15]. We assessed whether early fetal livers (E9.5 and E10.5) contain cells expressing these cell-surface markers (Fig. 1B). Livers derived from E9.5 to E13.5 mouse embryos were dissected and dissociated using collagenase. Cells were stained with antibodies against hematopoietic cell surface markers (CD45 and Ter119) as well as CD13 and Dlk. $CD13^+Dlk^+$ double-positive cells were found in the $CD45^-Ter119^-$ nonhematopoietic cell fraction derived from both early- and mid-fetal livers, although the expression level of CD13 and Dlk was low at E9.5 and increased during liver development. Liv2 is another cell surface molecule expressed on hepatic progenitor cells; numbers of Liv2-positive cells increase during E9.5 to E12.5 [8]. We found that $CD13^+Dlk^+$ cells in E9.5 fetal liver also expressed Liv2, indicating that cells expressing several hepatoblast cell-surface markers existed during early- to mid-fetal liver development (Supplementary Fig. S1). These results suggested that cell surface markers of hepatoblasts are commonly encountered during fetal liver development.

Phenotypic differences between early- and mid-fetal $CD13^+Dlk^+$ cells

To further characterize $CD13^+Dlk^+$ cells from each stage, expression of endodermal, hepatocyte, and cholangiocyte marker genes was analyzed using real-time RT-PCR. Strong expression of albumin and AFP was detected in $CD13^+Dlk^+$ cells derived from E13.5 mid-fetal liver (Fig. 2A). In contrast, these hepatocyte marker genes were detected at low levels in $CD13^+Dlk^+$ cells derived from E9.5 early fetal liver. Interestingly, E9.5 $CD13^+Dlk^+$ cells expressed CK19 and the early endodermal cell marker Sox17 at high levels (Fig. 2B). Although CK19 is known as a marker for cholangiocytes, it is also expressed in primitive gut endoderm at an earlier stage, including E9.0 [16]. Synthesis of albumin and CK19 was also analyzed using an in-droplet staining method (Fig. 2C). Although albumin levels were barely detectable in E9.5 $CD13^+Dlk^+$ cells, but they were accumulated during liver development. In contrast, CK19 expression levels in $CD13^+Dlk^+$ cells derived from E9.5 and E10.5 livers were higher than those in $CD13^+Dlk^+$ cells derived from E11.5 and E13.5 livers. These results indicate that gene expression patterns in early fetal $CD13^+Dlk^+$ cells are distinct from those in mid-fetal $CD13^+Dlk^+$ cells.

Proliferative capacity of $CD13^+Dlk^+$ cells derived from early- and mid-fetal livers

To analyze whether early fetal $CD13^+Dlk^+$ cells contain phenotypes of hepatic progenitor cells (exhibiting high proliferative potential and bipotency), we analyzed these cells using single-cell colony assays. Sorted single cells were inoculated into individual wells of 96-well collagen type I-coated culture plates. Cells derived from mid-fetal livers (E11.5 and E13.5) formed several small colonies (50–100 cells) and large colonies (over 100 cells) after 6 days of culture [13]. In contrast, cultures derived from E9.5 and E10.5 livers yielded few colonies or none (Supplementary Fig. S2). The nonhematopoietic cell fraction of E9.5 fetal livers comprises almost 1% $CD13^+Dlk^+$ cells and 99% $CD13^-$ or Dlk^- cells (Supplementary Fig. S3A). To exclude the possibility that early fetal progenitor cells are in the Dlk^- or $CD13^-$ fraction, we sorted 10,000 E9.5 fetal liver cells (100 $CD13^+Dlk^+$ cells and 9,900 $CD13^-$ or Dlk^- cells). Cells from neither fraction could form colonies in H-CFU-C culture medium on collagen-coated dishes. In addition, no colonies were detected in cultures derived from 10,000 nonsorted E9.5 liver cells, indicating that low colony-forming activities of E9.5-derived cells were not due to damage sustained during flow cytometry (Supplementary Fig. 3B). Nonsorted cells derived from E10.5 livers could form only a few small colonies but not large colonies (Supplementary Fig. 3C). Few colony formation of early fetal livers was also detected on gelatin-coated dishes (data not shown). These results suggested that conventional H-CFU-C culture on collagen- and gelatin-coated dishes is not suitable for early fetal (E9.5–10.5) HSPCs.

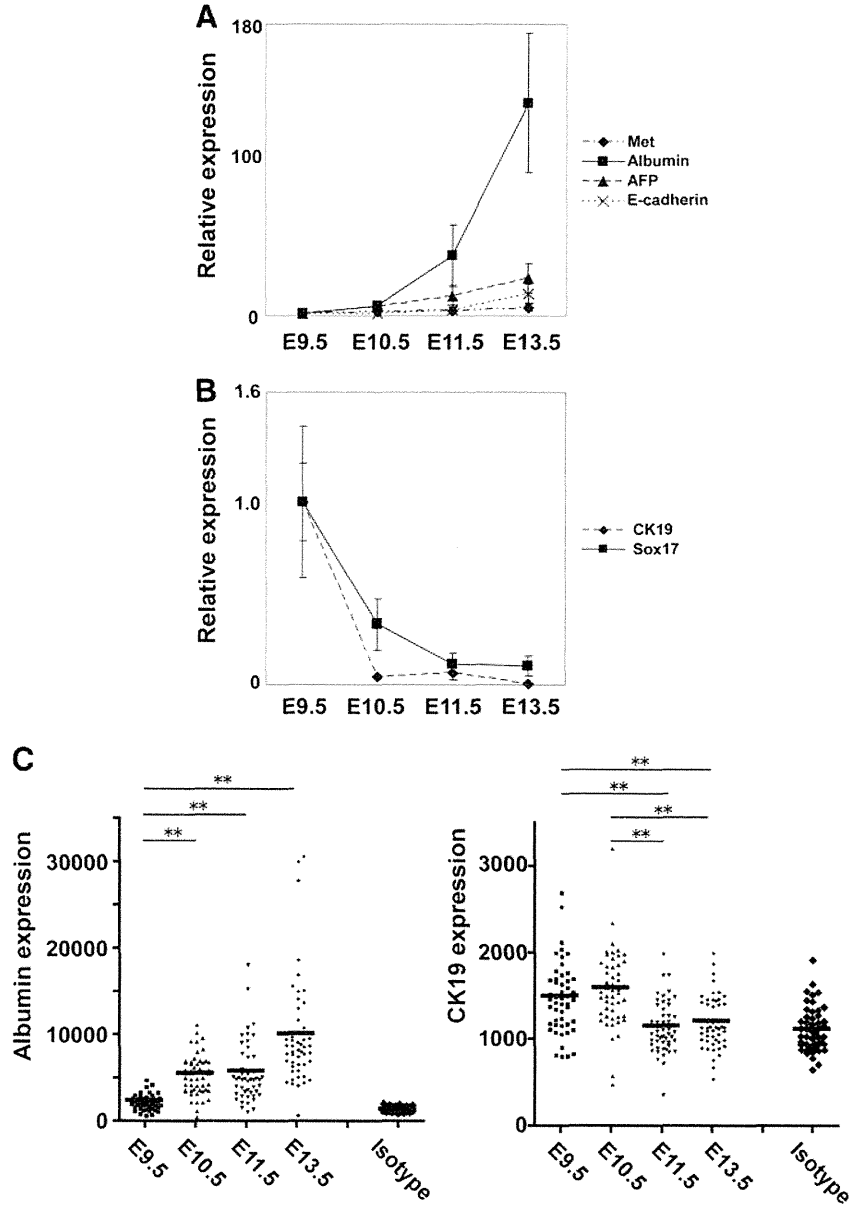

FIG. 2. Gene expression profiles of $CD45^-Ter119^-CD13^+Dlk^+$ cells during fetal liver development. **(A, B)** Expression of several hepatocyte (Met, albumin, AFP, and E-cadherin), primitive gut endoderm and cholangiocyte (CK19), and endodermal progenitor (Sox17) markers was analyzed using quantitative reverse transcription–polymerase chain reaction. $CD45^-Ter119^-CD13^+Dlk^+$ cells derived from E9.5, E10.5, E11.5, and E13.5 fetal livers were purified using flow cytometry. Expression level of marker genes in E9.5 cells was set to 1.0. Results are represented as relative expression ± SD (triplicate samples). **(C)** Protein expression (albumin and CK19) in $CD45^-Ter119^-CD13^+Dlk^+$ cells derived from E9.5, 10.5, 11.5, and E13.5 fetal livers. $CD45^-Ter119^-CD13^+Dlk^+$ cells were directly sorted onto slide glasses and were stained with primary antibodies (goat anti-albumin and rabbit anti-CK19 antibodies) and secondary antibodies (anti-rabbit IgG-Alexa488 and anti-goat IgG-Alexa546 antibodies). Results are represented as intensities of fluorescence of randomly picked-up cells ($n = 50$, $^{**}P < 0.01$). CK, cytokeratin; IgG, immunoglobulin G; AFP, α-fetoprotein.

Early fetal liver $CD13^+Dlk^+$ cells require both feeder cell interaction and the addition of ROCK inhibitor for their optimal expansion

Several studies have suggested that cell–cell interactions are important for proliferation and differentiation of somatic stem cells and progenitor cells. In early fetal liver development, the interaction between endodermal and mesenchymal populations is important for proper liver bud growth. Transcription factor Hlx, expressed in the septum transversum mesenchyme, is essential for proliferation of early fetal hepatic cells [17]. Therefore, we inferred that E9.5 $CD13^+Dlk^+$ cells need to interact with other cell populations to propagate both in vivo and in vitro. To mimic the interaction of hepatic and mesenchymal cells, $CD13^+Dlk^+$ cells were cocultured with MEF as mesenchymal feeder cells. We sorted either $CD13^+Dlk^+$ cells or other cells (Dlk^- or $CD13^-$ cells) in the nonhematopoietic cell fraction of E9.5 and E13.5 fetal livers. After 6 days of coculture with MEF, a few large colonies (containing both $albumin^+$ hepatocytic cells and $CK19^+$ cholangiocytic cells) were detected in culture of E9.5 $CD13^+Dlk^+$ cells (Fig. 3A). Some early fetal $CD13^+Dlk^+$ cells possess phenotypes of hepatic progenitor cells, *viz.*, high proliferative activity and bipotency. In contrast to mid-fetal hepatoblasts, early fetal HSPCs required interaction with mesenchymal fibroblasts for in vitro expansion. After 3 days of colony formation culture, early fetal $CD13^+Dlk^+$ cells expressed several hepatic genes and their expression levels were lower than those in mid-fetal $CD13^+Dlk^+$ cells, suggesting that early fetal cells are more immature types of progenitors (Supplementary Table S2). KSR is routinely employed in serum-free embryonic stem-cell culture protocols. We found that numbers of large and small colonies derived from E9.5 $CD13^+Dlk^+$ cells detected in KSR supplemented culture increased compared with those detected in FBS-supplemented culture (Fig. 3B). To explore signaling pathways regulating proliferation of early fetal liver